Masters Program in Geospatial Technologies

Groundwater Assessment and Monitoring in the Northeastern Part of Nigeria Using Microwave Remote Sensing

Oluwabukola Olufunke Akanbi

Dissertation submitted in partial fulfillment of the requirements
for the degree of Master in Master of Science in Geospatial Technologies

ifgi Institut für Geoinformatik Universität Münster
NOVA IMS Information Management School
init institute of new imaging technologies

Groundwater Assessment and Monitoring in the Northeastern Part of Nigeria Using Microwave Remote Sensing

Dissertation supervised by

Dr. Christian Knoth (Institut für Geoinformatik, University of Münster, Germany)

Prof. Roberto Henriques (NOVA Information Management School, Lisboa, Portugal**)**

Prof. Carlos Granell Canut (Department of Sistemas Informaticos, Universitat Jaume, Spain**)**

22nd February, 2023

Student ID
531420

Email: oakanbi@uni-munster.de

DECLARATION OF ORIGINALITY

I Oluwabukola Olufunke Akanbi declare that this Thesis Report is my own, unaided work. It is being submitted for the Master of Science at the University of Münster, Münster, Germany, Universidade NOVA de Lisboa, Lisbon, Portugal and Universitat Jaume, Castelló de la Plana, Spain. It has not been submitted before for any degree or examination at any other University.

Oluwabukola Olufunke Akanbi	22nd February, 2023
---	---
Name of candidate	Signature & Date

DEDICATION

I dedicate this paper to every region challenged with water supply crisis and doing all they can to keep the waters flowing while also creating systems of sustainability.

ACKNOWLEDGMENTS

I acknowledge the owner of all wisdom, the Lord God Almighty who strengthened and inspired my heart throughout my thesis period. My profound gratitude goes to my supervisor Dr. Christian Knoth of the University of Münster, Germany, for his guidance and resilience and always taking out time to explain and correct to the best of his knowledge. I am also grateful to my co-supervisors Prof. Roberto Henriques of NOVA Information Management School Lisbon, Portugal, who took out time to discuss my thesis with me and helped the best way he could, and Prof. Carlos Granell Canut of Universitat Jaume, Spain who called my project promising and helped the best he could. Additionally, i want to thank Prof. Pebesma Edzer of the University of Münster, Germany, for his constructive corrections and Tessio Novack for his guidance and attention throughout the thesis period.

I would also like to thank my dad, Engr. Isaac and mum, Mrs. Abosede, for their prayers and support. Super grateful to my siblings, you guys' rock! Lastly, I want to thank my colleagues, Lucas, Julia, Maryeme and Mareyam for their support and encouraging words.

ABSTRACT

As the human population continues to grow, the availability of surface water for convenient use is becoming increasingly scarce (Yu Fang et al., 2019). The negative effects of climate change such as drought has also been a major contributor to unavailability of surface water resources in certain regions (Brandon et al., 2017). Due to these reasons and more, natural reserves such as groundwater has become a primary and the most extensively used source of water (Brandon et al., 2017). The primary source of groundwater is gotten from precipitation, with a significant amount of precipitation in the presence of porous soils and with the help of gravity it infiltrates itself into the earth to form Groundwater, this in turn forms aquifers which can and has been harnessed over and over again through the construction of wells and boreholes and has been used for various purposes, including drinking, agriculture, and other human activities for centuries. Groundwater is also a key component of the water cycle; despite its invisibility it plays a crucial role in the ecosystem and the flow of various water bodies. Monitoring and investigating its variations and availability is therefore crucial for sustainability. Traditional methods such as geophysical and geo-electrical techniques have been utilized to detect, monitor and investigate groundwater resource for decades and have no doubt shown remarkable results, but these methods are not without limitations, they are expensive, time-consuming, and in some cases limited in spatial coverage, therefore optimization is necessary for progressiveness. New and more effective microwave-based techniques have been developed and realized in recent times, they have shown to be promising in handling complex hydrological investigations and observations, one of such technique is the Interferometric Synthetic Aperture Radar (InSAR), which utilizes Sentinel-1 satellite images to assess land surface deformation. This technique allows for mappings and investigations of groundwater variability over time in a particular region by studying the subsidence or uplift pattern which could be associated with groundwater recharge or depletion (Teije et al., 2018). Another important instrument for water management is the Gravity Recovery and Climate Experiment (GRACE) mission. GRACE measures global spatial mass changes caused by gravitational anomalies by using microwave k-band ranging sensor, accelerometers, and global positioning system receivers. GRACE is particularly important for water management as water has mass and its volume varies over time, because of this GRACE can identify and measure its variations. It is also the only satellite that can analyse Terrestrial Water Storage (TWS), which comprises of all the water storages on earth. Another technique worthy of mention is the Standardised Precipitation Evapotranspiration Index (SPEI), this index makes use of hydro-climatological parameters to estimate and investigate drought conditions in regions where it is integrated. Drought could occur due to seasonal and annual variabilities of precipitation and or temperatures which in turn can be as a result of climate change. Sentinel-1 and GRACE complement each other and have varying sensitivity to aquifer system change. This project employed data from both satellites to monitor and evaluate groundwater variability in the north eastern region of Nigeria. Also, due to unavailability of in-situ data for validations and results comparisons, I considered the hydro-climatology of this region and investigated the drought situation over the specified years to strengthen my findings.

List of Tables

List of Figures

List of Abbreviations

- Gravity Recovery And Climate Experiment Mission (GRACE)
- Global Land Data Assimilation System (GLDAS)
- Terrestrial Water Storage (TWS)
- Groundwater (GW)
- Microwave Remote Sensing (MRS)
- Persistent Scatterer Interferometric Synthetic Aperture Radar (PSInSAR)
- Standardised Precipitation Evapotranspiration Index (SPEI)
- United Nations International Children's Emergency Fund (UNICEF)
- Persistent Scatterers (PS)
- Water Table (WT)
- line Of sight (LOS)
- Stanford Method for Persistent Scatterers (StaMPS)
- Synthetic Aperture Radar (SAR)
- Digital Elevation Model (DEM)
- Single Look Complex (SLC)
- Sentinel Application Platform (SNAP)

Contents

CHAPTER ONE

1.0 INTRODUCTION

1.1 Background to the Study

The availability and distribution of water on the Earth's surface is a complex phenomenon that varies greatly. While a mere 3% of the surface water is fresh, the remaining 97% is saltwater. The majority of freshwater is retained in glaciers, and groundwater reservoirs accounts for about 29%, while lakes, rivers, and marshes comprise of less than 1% (Dr. Timothy.et.al, 2021). Given the increasing global population and negative effects of climate change, many nations have come to rely extensively on groundwater. Groundwater is a valuable natural resource that is stored in underground aquifers, which are porous rock formations and soil layers that can hold water. When precipitation falls on the ground, some of it is absorbed into the soil through a process called infiltration. As the soil becomes saturated, excess water begins to percolate downward through the soil and into the underlying aquifers. Over time, these aquifers can become large reservoirs of water that can be tapped into for a variety of uses, such as drinking water, irrigation, and industrial processes. Reports from the International Groundwater Acquisition Research Centre (IGRAC) in 2010, indicates that there has been a significant increase in groundwater abstraction and depletion in recent decades, with groundwater abstraction increasing from 312 to 734 km3 per year between 1960 and 2000, and groundwater depletion rising from 126 to 283 km3 per year, based on these statistics, IGRAC later concluded by saying “these trends are expected to continue in the future”. According to the Sustainable Water Partnership Activity report published by USAID in 2021, there is a projected 1% annual increase in global water demand over the next three decades. This demand is attributed to factors such as population growth, urbanization, and economic development. Additionally, climate change is expected to decrease surface water supply due to alterations in precipitation patterns, more frequent and severe droughts, and melting glaciers. As a result, groundwater resources may become increasingly critical as a source of water for various purposes. However, one example of a nation with abundant freshwater resources is Nigeria, which has a total of 286,200 MCM, with 23% of this coming from outside the nation. Nigeria's population of 210 million means that its renewable water supply of 1,499 m3/capita falls just short of the 1,500 m3/capita benchmark set by Falkenmark (USAID, 2021), but withdrawals are low (9.67 percent) and well below the SDG 6.4.2 water stress level. Regional water supply and demand however seem to be an issue, specifically, the northern region of the country experiences the highest water stress due to its location and natural climatological characteristics and also, water generally is not evenly distributed, therefore in this region, groundwater extraction is viewed as a potential solution (USAID, 2021). The sensitivity and cruciality of this recourse’s contribution to sustainability and stability of any viable nation calls for its

management and monitoring to avoid overuse and depletion. Groundwater is invisible, at least when it is under the ground and can be difficult to monitor, it is nonetheless crucial and worth exploring the complexities associated with monitoring it. Conventional methods of groundwater monitoring are based on the collection of direct measurements of water levels, hydrogeological studies, and chemical analysis of water samples, and this can be done using instruments such as steel tape, well dippers, sound devices, etc. (Amjad. et.al, 2022). These methods are relatively simple and have been used for decades to provide an understanding of groundwater resources. However, they are not without limitations; they can be costly, time-consuming and implementation area per-time can be restrictive. With the advancements in technology, modern techniques of groundwater monitoring have been developed and have shown promising results in recent times. Some of these techniques include Satellite-based Microwave Remote Sensing (MRS), groundwater modeling, and geophysical techniques. Satellite-based MRS offers a powerful and cost-effective method for monitoring groundwater resources, it uses microwave radiation to measure various properties of the Earth's surface and atmosphere. Microwave radiation has longer wavelengths compared to visible light, and can penetrate through clouds, dust, and other atmospheric obstructions, making it useful for remote sensing applications. Two Satellite-based MRS worthy of mention is Sentinel-1 and Gravity Recovery and Climate Experiment (GRACE) missions, they have shown to be relevant and promising in investigating variation in Terrestrial Water Storages such as groundwater. Sentinel-1 is able to detect land deformation due to its ability to penetrate clouds and acquire Synthetic Aperture Radar (SAR) images, to achieve this, it utilizes techniques one of which is the Persistent Scatterer Interferometric Synthetic Aperture Radar (PSInSAR) which uses SAR images to detect surface movements and ground displacement by using stable scatterers or reflectance. These land movements could be due to groundwater depletion or recharge in any area it is implemented (Teije et al., 2018). The GRACE mission uses a pair of satellites that orbit the Earth in tandem, constantly measuring the distance between them with high precision. The distance between the satellites changes as they fly over areas of varying gravity, caused by variations in the Earth's mass such as changes in water storage, ice sheets, and snow cover. GRACE when combined with hydrological frameworks such as GLDAS can estimate individual TWSs such as Soil Moisture, Canopy Water, Groundwater, etc. Another technique that focuses on climatology and assesses its effects on TWS is the Standardised Precipitation Evapotranspiration Index (SPEI), it investigates the drought situation in a specified region and checks its severity and frequency. A combination of these three techniques can help provide a comprehensive understanding of the current state and future conditions of groundwater or aquifer system in a specific region, which is crucial for sustainable water resource management (Sahaj, 2020). In chapter3, I have explained in details these individual techniques.

1.2 Problem Statement

According to UNICEF Representative in Nigeria, Peter Hawkins, "Our world is facing a water crisis, and children are its biggest victims". Groundwater (GW) makes up 99% of usable freshwater and complements for seasonal and annual variabilities of surface water, monitoring is therefore crucial in order to contribute to the research on sustainable water systems. Particularly in my areas of interest, groundwater is the main source of irrigation and municipal purposes for rural and urban areas. A rise in water demand could bring about declining groundwater levels which could contribute to water stress in this region and hamper the access to water for vulnerable populations. Other factors such as climate change could also be a contributing factor. Conflicts and policy instability are also being caused by increasing competition over land and water resources between pastoralists and farmers.

1.3 Aim, Objectives and Research Questions

Aim

Investigate how land deformation inferred from sentinel-1 and groundwater anomaly inferred from GRACE indicates change in ground water levels in the Northeastern part of Nigeria.

Objectives

1. Analyse land deformation by the means of spatial-temporal deformation map derived through Persistent Scatterers (PS).
2. Investigate the variation in groundwater storage in the region using GRACE.
3. Investigate the drought situation in this region using SPEI
4. Compare Sentinel-1 results, GRACE results and SPEI results to observe temporal trends for similarities and validations.

Research Questions

1. How can GRACE be used to monitor groundwater changes in the North-eastern part of Nigeria?
2. Observing the results from Sentinel-1 and GRACE, can we conclude that land deformation has a similar trend?
3. How can we combine the results from GRACE, Sentinel-1 and SPEI to monitor the groundwater situation in higher (spatial) detail in the study area?

1.4 Thesis Structure

This thesis report begins with the abstract by giving a brief summary of the research, then **Chapter 1** starts by presenting a brief explanation of water statistics and the significance of water in general. Subsequently, the report highlights the importance of groundwater and mentions the various methods used to monitor it. Thereafter, are the presentation of the research aims, objectives, and questions.

Chapter 2 starts and ends with briefly highlighting and summarizing papers that have been written by other researchers on the same topic and with a similar methodology.

In **Chapter 3**, I introduce the study area along with the data and tools that I have obtained and utilized for analysis. Furthermore, I provide a comprehensive explanation of the specific techniques that I have employed to achieve my goals and objectives. The chapter also features methodological flowcharts that demonstrate the process chain-line for individual technique.

Chapter 4 of the report presents and discusses all of the results and validations obtained from my study which includes Land Deformation, Groundwater Anomaly and Standardised Precipitation Evapotranspiration Index (SPEI). In this section, I delve into the findings in detail and provide a thorough analysis of the results in maps and graphical representations.

Moving on to **Chapter 5**, it serves as the concluding chapter of the report. In this section, I summarize the key results obtained from the study and highlight any limitations that may have impacted the study's findings. Additionally, I identify potential areas for future research in the field.

In addition to the main body of the report, the **References** and **Appendix** sections provide further information and resources related to the study. The References section includes a list of all the sources cited throughout the report, while the Appendix section includes additional materials, such as tables, graphs, figures, and supplementary data, that support and enhance the findings presented in the main body of the report.

1.5 Scope of Thesis

Please note that this project did not consider the different aquifer types (confined and unconfined) and was mainly concerned with general groundwater variations. This project did not also entail in-depth statistical estimations as validations were based on observance of realised temporal variation trends from Land Deformation, Groundwater Anomalies and SPEI.

CHAPTER TWO

2.0 LITERATURE REVIEW

Zhen Liu et al., (2019) conducted a study in California's Central Valley over a period of three years (2015-2017) to monitor changes in groundwater levels. The region heavily relies on groundwater resources for urbanization and agricultural usage, and over-utilization coupled with droughts have caused a significant decline in groundwater levels over the past century. The authors used data obtained from Sentinel-1 and Gravity Recovery and Climate Experiment Mission (GRACE) to analyse land deformation induced by groundwater pumping and to derive groundwater anomalies. They found a steady subsidence in the study area over the specified years, and a temporal depletion in groundwater resources. The study also observed a strong correlation between land subsidence and groundwater depletion, which was further validated by in-situ well records and found to be true, they attributed these variations to excessive groundwater pumping for farming and irrigation. Rakesh et al., 2019, utilized data from Sentinel-1 and GRACE satellites to map changes in groundwater storage in the Indian states of Gujarat and Rajasthan. According to their research, the state of Rajasthan experienced a substantial decrease in groundwater storage, equivalent to around -4.17 km3 per year, from 2002 to 2016, primarily due to excessive extraction for irrigation. Conversely, Gujarat recorded an increase in groundwater storage, approximately 1.76 km3 per year, during the same period. In Tulare Basin, California, Donald et al. (2018) utilized data from Sentinel 1 and GRACE satellites to observe hydrological changes in confined and unconfined aquifers, and then verified their results using in-situ well data. According to their research, the overlying unconfined aquifer at the eastern edge of the Central Valley displayed an increase in volume in March 2019, which they attribute to a combination of preceding winter rains and early snowmelt. Meanwhile, in the confined aquifer, a northwest-oriented volume increase was observed in the Central Valley region, following the deeper portion of the aquifer, and this increase was linked to water inflow from rivers, mainly in the southern Sierra Nevada and the northern region. The findings from the in-situ well data also support the increase in groundwater volume in this area, which aligns with the GRACE trends observed in the study. Teije et al., 2018 carried out research in Yangon, Myanmar using Sentinel-1 persistent scatterer interferometry to monitor land subsidence and assessed its driving mechanisms. According to their report, they stated that responsible authorities supply water to less than half of the city using reservoir water and pipes, which accounts for 10% of groundwater. The rest of the inhabitants depend on groundwater extractions for their water supply, and even those who receive water from the water authorities also rely on groundwater when water supply is unavailable. Based on their PSI results, they were able to demonstrate that more than half of Yangon is experiencing subsidence at rates exceeding 10 mm/yr. between December 2014 and April 2017. They also stated that during this

period, the aquifer system lost a storage volume of 13 million cubic meters. Further on, four locations with significant subsidence velocities exceeding 20 mm/yr., which accounted for 15% of the total data points was identified, two of which were located in previously agricultural areas that have been incorporated into the city over the last thirty years. They concluded that If groundwater extractions are not addressed, Yangon may become more susceptible to infrastructure damage, flooding events, and a decline in the quality of the aquifer. Using Sentinel-1 data and the SNAP-StaMPS Persistent Scatterer Interferometry technique, José et al. (2019), conducted a study to assess urban subsidence in the Rome metropolitan area (Italy). The researchers observed diverse deformation patterns in the area, with one of the most prominent being subsidence at Fiumicino airport at a rate of -20 mm/yr. Additionally, motion along the Tiber River and its tributaries was measured to be around -5 mm/yr. The researchers validated their findings by comparing them with previous studies and attributed the subsidence occurrences to local geological conditions, such as the compaction of soft sediments possibly resulting from groundwater depletion. However, they also noted that the weight of urban constructions could be one of the primary reinforcing factors. Brandon et al. (2016) evaluated the impact of drought on groundwater resources in the Marshall Islands by examining the hydro-climatological patterns of the region. Using an algebraic model designed for atoll islands, they analyzed average seasonal rainfall and drought conditions. The researchers found that the groundwater resources in the Marshall Islands are extremely fragile, with groundwater on most islands <300m in width becoming completely depleted during drought periods. Only larger islands >800m were able to maintain a sizeable freshwater lens for use by the population. Vanesa et al., (2020), used SPEI in predicting water table dynamics in Argentinian plains. Their studies proofed that water table behavior can be predicted from climatological indices such as rainfall patterns and temperature used for SPEI estimation, they however did not calculate SPEI but acquired it and validated it with Water Table (WT) data acquired from authorized stations. Jipkate et al., (2020) estimated drought Indices for assessing the impact of climatic variables on groundwater fluctuation over upper Bhima Sub Basin. They estimated both SPEI and Standardized Precipitation Index (SPI) using Temperature and Precipitation, the spatial variations in meteorological drought in the specified region appears to be random, with groundwater levels changing and moving west to east and south to north and vice versa. According to their report they stated that a major cause of drought is rainfall deficit.

CHAPTER THREE

3.0 MATERIALS AND METHODS

3.1 Study Area

Maiduguri is situated in two Local Government Areas in the northeastern state of Borno, Nigeria - Maiduguri and Konduga. The village of Marraraba, on the other hand, is located in Hong Local Government Area in Adamawa state, which is also situated in the northeastern region of the country. Both areas are characterized by a semiarid climate (BSh), with relatively low annual rainfall that occurs over a short period of three to four months (June-September). The weather is usually hot and dry throughout most of the year, and temperatures reaching highs of up to 40 °C (104.0 °F) have been recorded (Abubakar Ibrahim, 2012).

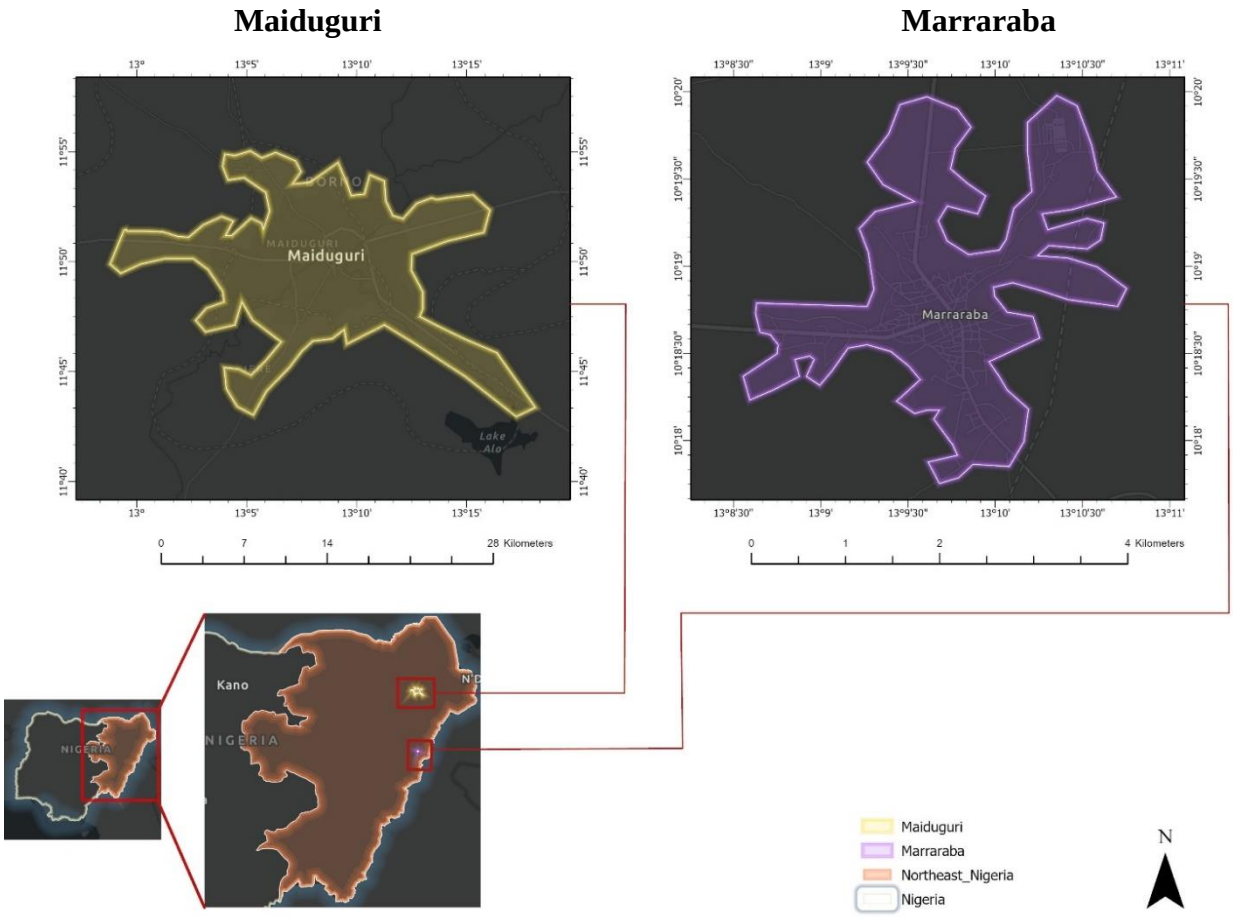

Figure (1) Map showing the two areas of interest (Maiduguri and Marraraba).
Source: author

The main occupation of people in these two regions is Agriculture and it is largely dominated by the Hausa, Fulani and Nupe speaking tribe. Maiduguri has a landmass of 105.5 km² and has a population of 786,000 as of 2019, while the landmass of Marraraba is 1.677 km² and has a population of 1,141 as of 2015 (Abubakar Ibrahim, 2012).

3.2 Data used for analysis

For this Thesis I have used GRACE and Sentinel-1 missions, GLDAS Hydrological Assimilation Framework, Precipitation and Temperature. Data were acquired from secondary sources;

- **Sentinel-1** data was obtained from Alaska Satellite Facility website: https://search.asf.alaska.edu/#/
- **GRACE** data was obtained from The University of Texas at Austin website: https://www2.csr.utexas.edu/grace/RL06_mascons.html.
- **GLDAS** was obtained from NASA Earth Data https://disc.gsfc.nasa.gov/datasets?keywords=GLDAS.
- **Precipitation** and **Temperature** were obtained from NASA Prediction of Worldwide Energy Resources website: https://power.larc.nasa.gov/data-access-viewer/
- Other datasets used includes; The Nigeria Shapefile gotten from GADM Maps: https://gadm.org/download_country.html.

The table below shows the different datasets in detail.

S/N	***Data***	***Product***	***Spatial Resolution***	***Temporal Coverage***	***Temporal Coverage Used in Study***	***Format***
1.	Sentinel-1	SLC Ascending	5m	6 - 12 days	2019 - 2021	Raster
2.	GRACE	Mascon	0.25° x 0.25°	Monthly	2019 - 2021	Raster
3.	GLDAS	NOAH Land Surface model	0.25° x 0.25°	Monthly	2019 – 2021	Raster
4.	Shapefile	GADM	-	-	-	Vector
5.	Precipitation	NASA power	1° x 1°	Monthly	2019 – 2021	CSV
6.	Temperature	NASA power	1° x 1°	Monthly	2019 – 2021	CSV

Table (1) Data used for analysis

Tools and Application Used

✓ ArcGISPro	✓ Python 2.7 and 3.8	✓ Qgis
✓ MATLAB	✓ SPEI App	✓ SNAP
✓ Excel	✓ aria2c	✓ Lucid

Table (2)

3.3 Sentinel-1 Mission

Sentinel-1 is a European Space Agency (ESA) satellite mission that provides radar imaging data for a variety of applications, including land and ocean monitoring, disaster management, and maritime surveillance. Sentinel-1 uses microwave frequency (C-band) Synthetic Aperture Radar (SAR) to image the earth surface. SAR is an active remote sensing technology that sends microwave pulses to the earth's surface and measures the backscattered signals to create images.

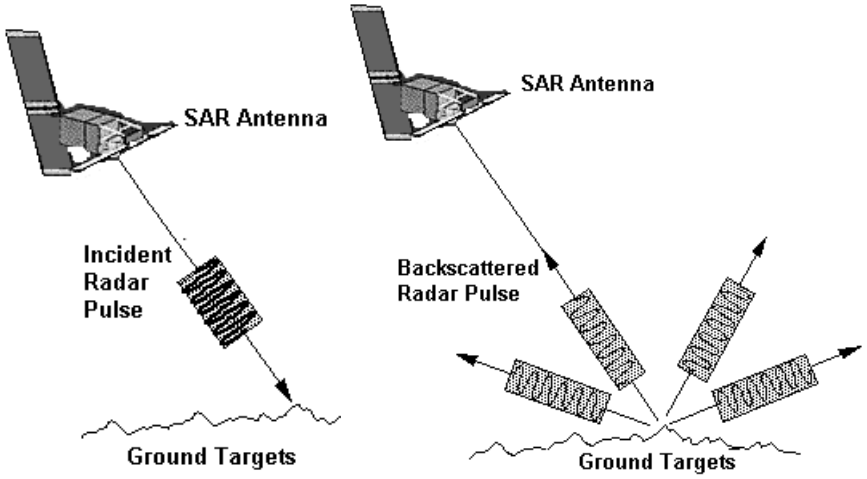

Figure (2) Image representing Radar Pules Transmission and Backscatter
Source: https://crisp.nus.edu.sg/

The C-band radar has a wavelength of about 5.6 cm, allowing it to penetrate through clouds and darkness to capture detailed images of the earth's surface (Torres et al., 2012). The mission is composed of two identical satellites, Sentinel-1A and Sentinel-1B, which together provide a revisit time of 6 to 12 days at the equator. The resolution of Sentinel-1 images varies depending on the imaging mode used by the satellite. In spotlight mode, Sentinel-1A and Sentinel-1B can acquire images with a resolution of up to 1 meter. This mode is used for high-resolution mapping of small areas. In stripmap mode, the resolution is around 5-10 meters and it's mainly used for monitoring of large areas (ESA SP-1322/1 Sentinel-1, 2012). In wide-swath mode, the resolution is around 20-40 meters and it's mainly used for large scale mapping and monitoring (ESA User Guides).

One of the key applications of Sentinel-1 is in Land Deformation mapping; which could be as a result of groundwater depletion (Teije et al., 2018). Groundwater is a vital resource for many regions around the world, providing drinking water for rural and urban communities, irrigation for agriculture, and maintaining the health of ecosystems. However, groundwater is a vulnerable resource, as it is often depleted faster than it can be replenished. Conventional methods of monitoring groundwater, such as drilling wells, sounding devices and measuring water levels, are often costly, time-consuming, and not always reliable when investigating large areas. Sentinel-1 in combination with Gravity recovery And Climate Experiment Mission (GRACE) provides an innovative solution to this problem by using Microwave-based sensors to monitor groundwater changes. The radar system can measure the surface deformation which could have been caused by changes in the water table, allowing scientists to estimate the changes in groundwater storage (Vasco et al., 2022). With this vital information, water managers can make more informed decisions about how to manage the groundwater resource.

In SAR measurement, there are two measurable quantities, namely the amplitude and phase signals. The amplitude signal is related to the electrical properties, orientation, and shape of the target, and it represents the strength of the backscattered electromagnetic wave or radar brightness. On the other hand, the phase signal measures the differences in distance between two or more SAR images from the sensor to the ground target, and it varies from $-\pi$ to $+\pi$ for every wavelength of distance traveled. The phase signal is used to form an interferogram, which is a representation of the differences in distance between two SAR images, this whole concept is known as Interferometry Synthetic Aperture Radar (InSAR). Furthermore, it's possible for a fringe to appear in an interferogram, indicating the displacement of a ground pixel in the line of sight (LOS) direction (Yan Akhbar, 2021). The image on the left shows a representation of a phase shift. The satellite acquires SAR image over a specified area and at a specified time for the first time, then it acquires another image a second time over the same location but at a different time, if there is a phase shift it is then recorded and interpreted as an interferogram as initially explained.

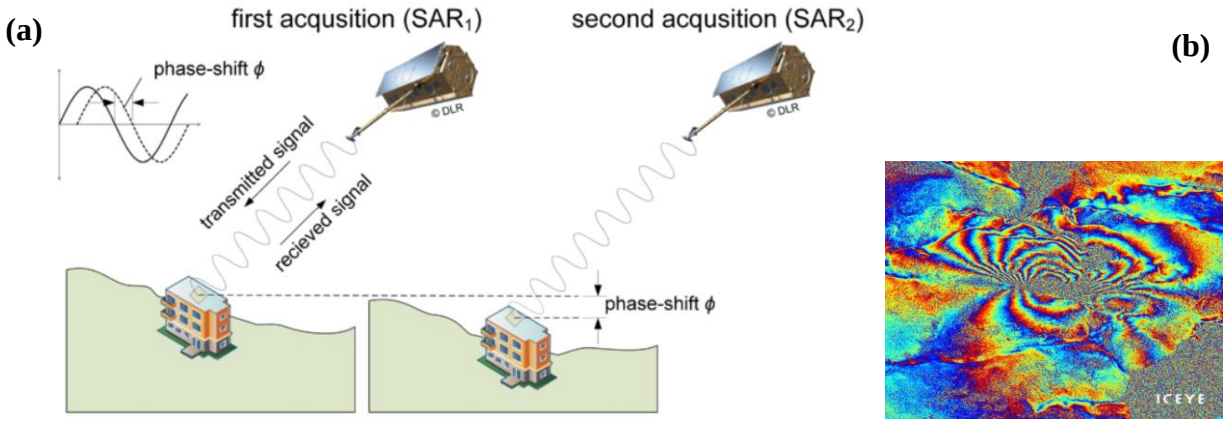

Figure (3) Image representing Phase-shift (a) and Interferogram (b)
Source: https://crisp.nus.edu.sg/

The change in signal phase ($\Delta\varphi$) can be expressed as: $\Delta\varphi = 4\pi/\lambda * \Delta R + \alpha$
Where λ is the wavelength, ΔR is the displacement in the Line Of Sight (LOS), α is a phase shift due to different atmospheric conditions at the time of two radar acquisitions, and the factor of 4π converts the LOS displacement to a phase shift in radians. For Land Deformation analysis, a number of Interferometry Synthetic Aperture (InSAR) techniques have shown effective and promising results, some of which include; Multi-Temporal Interferometric Synthetic Aperture Radar (MTInSAR), Small BAseline Subset (SBAS), Differential Interferometric Synthetic Aperture Radar (DInSAR), and Persistent Scatterer Interferometric Synthetic Aperture Radar (PSInSAR).

For my analysis, I utilized the Stanford method for Persistent Scatterers (StaMPS) which is a form of PSInSAR. The advantage of using this technique is that it allows for the mapping and investigation of widespread deformation trends with a high level of accuracy, up to sub-centimeter precision, and on a dense grid (Ferretti et al. (2001); Sousa et al. (2011)). StaMPS is used in radar interferometry to identify stable points on the Earth's surface, called persistent scatterers (PS), they can be used to measure land surface deformation with high precision. This method uses radar images acquired by satellites, such as the European Space Agency's Sentinel-1, to detect and track PS over time, which can in turn be used to map land deformation and investigate changes in groundwater levels. The analysis commences within the Sentinel Application Platform (SNAP) environment. SNAP is a software framework that provides users with the ability to process and analyze data with respect to their objectives, specifically in the case of this thesis, SAR data. Snap2StaMPS is a software package that is used to automate the process chain line for the StaMPS method in the SNAP environment, it was specifically designed to optimize the StaMPS technique.

3.3.0 PSInSAR and StaMPS

The PSInSAR technique relies on identifying permanent or persistent scatterers (PSs), which are pixels with a single dominant point scatterer that exhibit coherence throughout the entire time-series of observations, effectively minimizing decorrelation phase noise. Some examples of PSs as seen in figure (3) include buildings, roads, rocks, etc., whose reflectivity remains stable over time. As a result, a significant stack of SAR images is necessary to identify dependable PS points. (Hooper et al., 2006; Din et al., 2015). The Stanford Method for Persistent Scatterers (StaMPS) is a software package that incorporates a PSInSAR method, enabling the detection of terrain deformation in regions that are deficient in human-made structures or display non-steady deformation. It provides a potent means for analysing the movement and deformation of natural components, such as rocks and vegetation, over

extended periods. As mentioned, these movements are known as phase shift and can be recorded and interpreted as interferograms (StaMPS Manual, Version 4.1b, Andy Hooper. et. al, 2018).

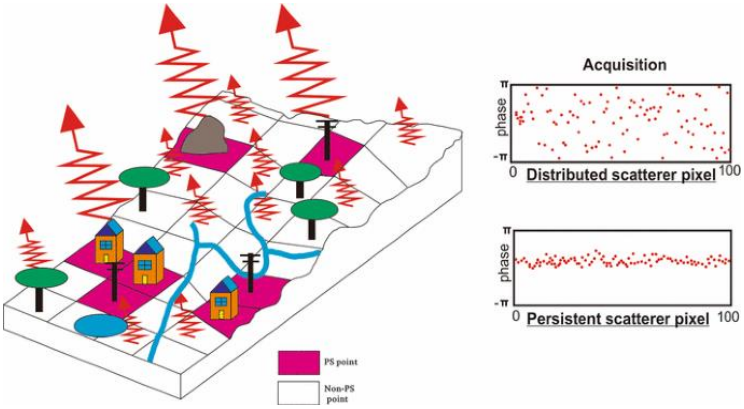

Figure (4) Image representing Persistent Scatterers
Source: https://crisp.nus.edu.sg/

StaMPS and its associated tools have found diverse applications, such as monitoring landslides, subsidence, and volcanic activity, and have demonstrated their efficacy in analysing natural phenomena that affect the Earth's surface. The ability of StaMPS to operate in areas that lack man-made structures or exhibit non-steady deformation is particularly valuable, and the incorporation of the small baseline method and multi-temporal InSAR approach in StaMPS/MTI further enhances its utility in analysing complex natural processes. (StaMPS Manual, Version 4.1b, Andy Hooper. et. al, 2018). StaMPS comprises of 8 steps; these steps can be run individually (i.e., stamps (1,1)) or collectively (i.e., stamps (1,8)). The notation "stamps (1,1)" refers to a single step in the processing pipeline, where the first "1" represents the starting step and the second "1" represents the ending step. However, depending on the available processing power of the machine, it may be possible to run multiple steps at once. This means that instead of running a single step at a time, multiple steps can be executed concurrently, potentially reducing the overall processing time. (StaMPS Manual, Version 4.1b, Andy Hooper. et. al, 2018).

3.3.1 How StaMPS work during implementation

The following steps attempts to explain what each steps do and how to run it. Please not that MATLAB is required to run these steps.

STEP 1: Initial load of data

The first step involves loading the data for the initial candidate PS pixels and saving them as MATLAB workspace files. To execute this step, you simply type: stamps (1,1).

STEP 2: Calculate temporal coherence by estimating phase noise

This process is iterative and involves estimating the phase noise value (γ) for each potential pixel in all the interferograms (as described in the StaMPS manual). To execute this step, you simply type: stamps (2,2).

STEP 3: Select PS pixels

This step entails selecting Persistent Scatterers (PS) that are likely based on a probability comparison to results obtained from data with random phase. This selection process is carried out twice. After the first selection, the temporal coherence of each chosen pixel is more accurately re-estimated by excluding the pixel itself from the estimation of the spatially correlated phase. Following this, the selection process is repeated (A. Hooper in 2018). To execute this step, you simply type: stamps (3,3).

STEP 4: PS weeding

Next, in the process, the previously selected pixels undergo screening and pruning, with any that are found to be as a result of signal contributions from neighbouring ground resolution elements or deemed excessively noisy are excluded. The data for the remaining selected pixels is then stored in new workspaces. (StaMPS Manual). To execute this step, you simply type: stamps (4,4).

STEP 5: Phase correction

The selected pixels then undergo a correction process in which their wrapped phase is adjusted to account for any spatially uncorrelated look angle (DEM) error (StaMPS Manual). To execute this step, you simply type: stamps (5,5).

STEP 6: Phase unwrapping

The measurement of phase is typically limited to the range of 0 to 2π. Given the relationship between phase and wavelength, it's evident that several 2π cycles can occur before the signal reaches the ground, especially considering that the wavelength used for Sentinel-1 is 5.5 cm. As a result, the interferometric phase difference at any point can be between 0 to 2π plus an unknown number of cycles (k). Phase unwrapping calculation, also known as the process of reconstructing the original phase shift from this "wrapped" representation, is used to address this phase ambiguity. The calculation involves adding or subtracting multiples of 2 in appropriate places to smooth out the phase image as much as possible. In this step, the unwrapping process is performed by StaMPS using the software tool "snaphu". (StaMPS Manual). To execute this step, you simply type: stamps (6,6).

STEP 7: TRAIN - Linear tropospheric correction is run before running step 7

Since the phase and topographic information are realized at this stage, the linear tropospheric correction can be computed using TRAIN. (StaMPS Manual, Version 4.1b, 2018). To execute this step, you simply type: aps_linear.

STEP 8: Calculate spatially correlated look angle (DEM) error

In this step, errors in the digital elevation model (DEM) and its mapping into radar coordinates are calculated, along with the simultaneous estimation of the phase associated with master atmosphere and orbit errors (AOE). To execute this step, you simply type: stamps (7,7).
For further comprehensive understanding on the StaMPS steps, please refer to StaMPS Manual, Version 4.1b, written by Andy Hooper. et. al, 2018.

3.3.2 Pre-processing of SAR images in SNAP Environment

After setting up my machine by installing and downloading the necessary packages and software, I acquired my SAR data as illustrated in figure (6), the SAR images were then loaded into the SNAP environment, then the master image was selected. A master image is a single radar image that is used as a reference for creating interferograms. Usually, the master image is selected because it offers the best quality, has the least amount of noise, and is geocoded, which means it's precisely located in geographic coordinates. These features make the master image ideal as a reference image to align and compare other images accurately for phase shift measurements. After the master image was selected then I selected my area of interest as seen in figure (7) and (8) using the graph (figure (5)) below because Sentinel-1 SLC image is formed by several bursts:

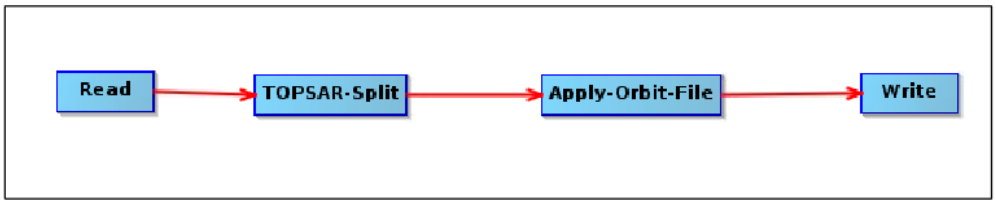

Figure (5) Graph representing splitting and orbit

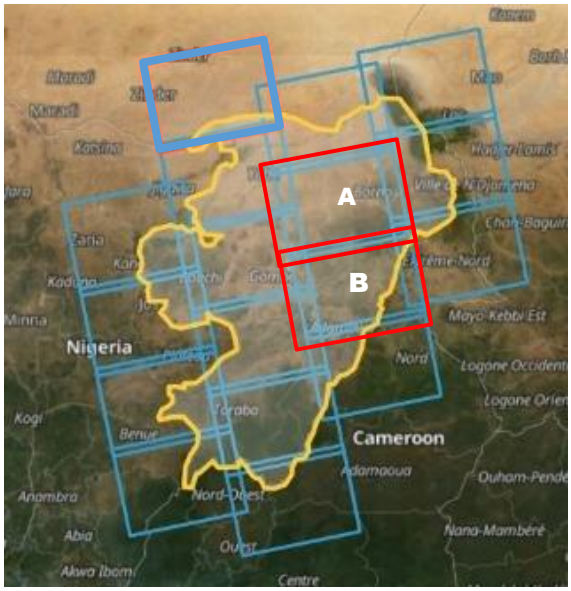

Figure (6). Selected footprints where the areas of interest are located.

The labelled footprints correspond to where my selected regions of interest are located.

- Maiduguri is located in footprint “A”, It is an urban settlement situated in Borno State, Nigeria, with a landmass of 105.5 km².
- Marraraba is located in footprint “B”, it is a rural settlement located in Adamawa State, Nigeria, with a landmass of 1.677 km².

Maiduguri “A”, the first region

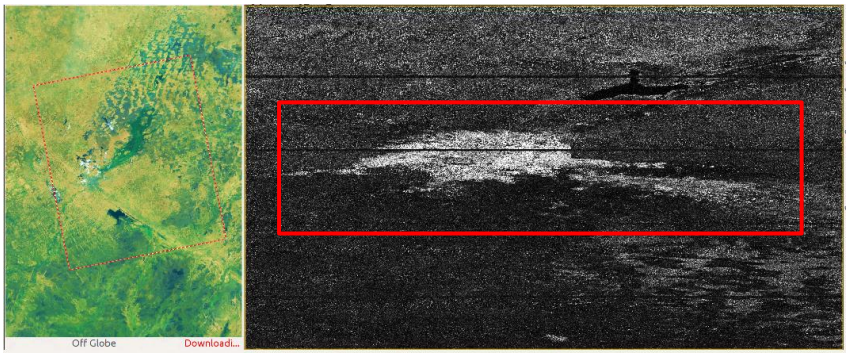

Figure (7). Sentinel-1 image and footprint of Maiduguri
Source: author

Marraraba “B”, the second region

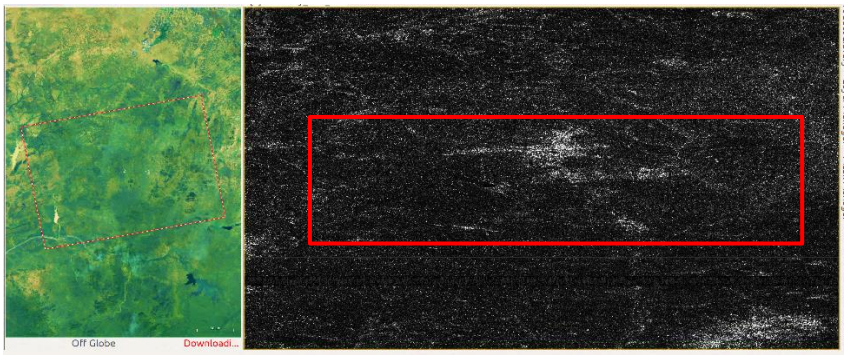

Figure (8). Sentinel-1 image and footprint of Marraraba
Source: author

The rest of the preprocessing as seen in flowchart (1) were actualized using **snap2StaMPS**.

3.3.3 snap2StaMPS software package used to automate SAR image pre-processing

snap2StaMPS is a Python-based process designed by José Manuel Delgado Blasco and Michael Foumelis in partnership with Prof. A. Hooper. Its purpose is to optimize the pre-processing of Sentinel-1 SLC data and facilitate their conversion for use in StaMPS. For single master interferograms compatible with StaMPS PSI. snap2stamps includes a collection of graphs and python wrappers that let you automate the interferogram processing chain. I have listed below the flies that can be found in this package and their functions:

- **project.conf** – file with parameters and paths needed for the processing

```
######### CONFIGURATION FILE #####
###################################
# PROJECT DEFINITION
PROJECTFOLDER=/application/wokdir/PROC
GRAPHSFOLDER=/application/workdir/GRAPH
###################################
# PROCESSING PARAMETERS
IW1=IW2
MASTER=
###################################
# AOI BBOX DEFINITION
LONMIN=
LATMIN=
LONMAX=
LATMAX=
###################################
# SNAP GPT
GPTBIN_PATH=/application/pi/snap/bin/gpt
###################################
# COMPUTING RESOURCES TO EMPLOY
CPU=8
CACHE=16G
###################################
```

Figure (9) Image showing configuration file
Source: author

- **slaves_prep.py** – script for slave sorting in the expected folder structure

- **splitting_slaves_logging.py** – script for slave splitting (and assembling is needed) and orbit correction and its corresponding graph.

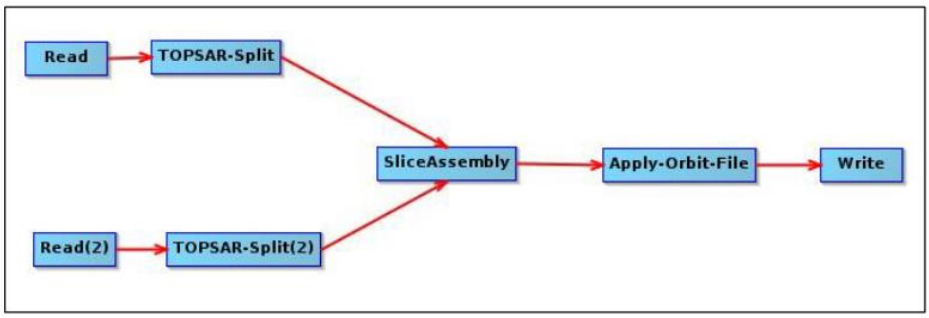

Figure (10) Graph representing Split-Slice Assemble and Apply Orbit
Source: author

- **coreg_ifg_topsar.py** – script for master-slave co-registration and interferometric generation and its corresponding graph.

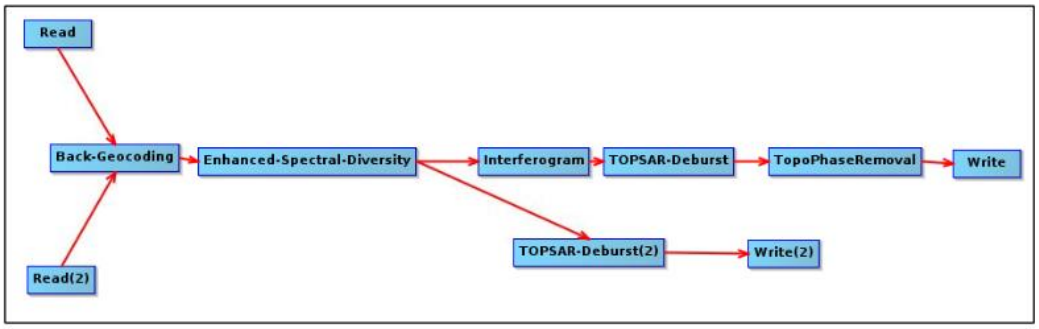

Figure (11) Graph representing Co-registration and Interferogram generation
Source: author

- **stamps_export.py** – script for output data generation in StaMPS compatible format for PSI processing and its corresponding graph.

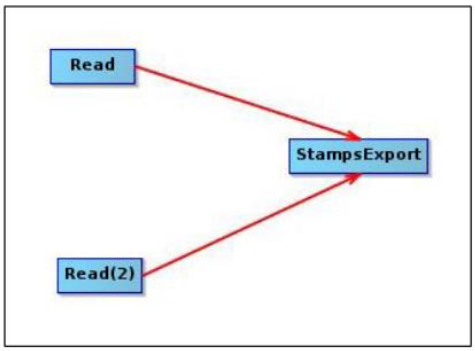

Figure (12) Graph representing StaMPS export
Source: author

For further comprehensive understanding, please refer to SNAP2StaMPS_User_Mannual, Version 1.1, written by José Manuel Delgado Blasco and Michael Foumelis.

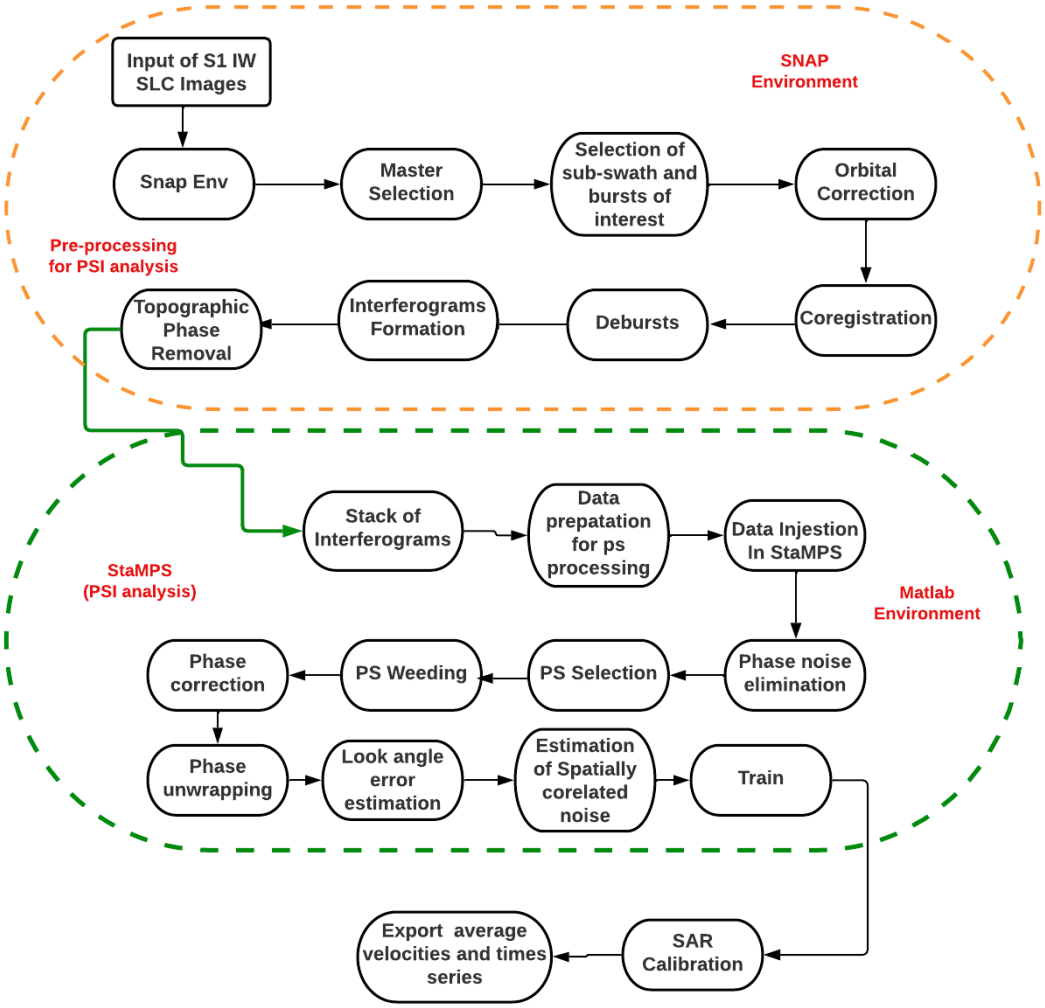

Figure (13) Flowchart-1 for Land Deformation Analysis
Source: author

3.3.4 Gravity Recovery and Climate Experiment (GRACE) Mission

GRACE mission is a satellite-based gravity measurement system that was launched in 2002 by NASA and the German Aerospace Center (DLR). It comprises of two identical satellites, GRACE-A and GRACE-B which are flown in tandem approximately 220 km apart (NASA; JPL, updated - 2022).

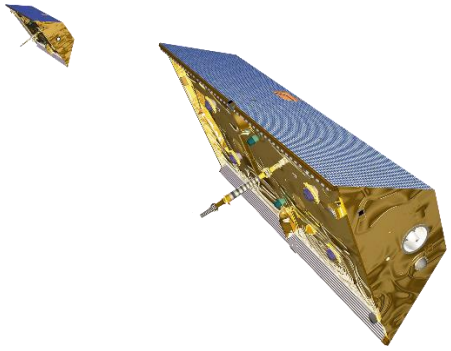

Figure (14) GRACE Satellite Mission
Source: https://en.wikipedia.org/wiki/GRACE_and_GRACE-FO

The distance between the two satellites is precisely measured by a microwave ranging system, and the relative acceleration of the two satellites is measured by a set of accelerometers. The mission's primary goal is to measure variations in the Earth's gravity field with high precision and accuracy using a technique called gravity gradiometry. These variations are caused by changes in the distribution of mass on the Earth's surface, such as changes in the water storage in aquifers, ice sheets, and glaciers. One of the key applications of the GRACE data is in the field of hydrology, specifically in the monitoring of Terrestrial water resources which is crucial for sustainable water resource management, as it allows for the assessment of the effects of different management scenarios and the prediction of future conditions (NASA; JPL, updated - 2022). The data from GRACE can be used to estimate the individual total water storage changes through and with the combination of modeling and data assimilation frameworks such as Global Land Data Assimilation System (GLDAS), so as to separate and estimate the contributions of different water storage components such as soil moisture, surface water, and groundwater. GRACE has shown promising and effective results where it has been used to monitor and investigate water resources in a number of regions. One of the advantages of using GRACE data is for groundwater monitoring, its high temporal resolution, with measurements taken every 30 days allows for the detection of short-term variations in the groundwater storage and the estimation of the recharge and discharge processes. Additionally, GRACE data has a relatively high spatial resolution of about 300km, which allows for the monitoring of regional-scale and or global-scale groundwater resources (NASA; JPL, updated - 2022). The mission is a powerful tool for understanding the Earth's gravity field and the changes in the distribution of mass on the Earth's surface. A few products or data are realized from GRACE, and the product I have acquired and used for my analysis is called Terrestrial water storage (TWS), this refers to the amount of water stored on and beneath the ground, such as glaciers, snow, lakes, rivers, and groundwater aquifers. The TWS data is in an anomaly format with an anomaly baseline of 2004 to 2009. The equation below shows all compartment of storages contained in the TWS; this however depends on the Hydro-climatology of a specified region of interest.

$$\Delta \text{TWS} = \Delta \text{SM} + \Delta \text{GWS} + \Delta \text{SWE} + \Delta \text{CWS} + \Delta \text{SW}$$

- Δ SM: Soil moisture anomaly
- Δ GWS: Groundwater Storage anomaly
- Δ SWE: Surface water or Surface Runoff anomaly
- Δ CWS: Canopy Water anomaly
- Δ SW: Snow Water anomaly

The image below shows Global TWS (Product: csr/grace/RL06_mascons) from 2004 to 2022, with each band representing monthly timestamp. This data has been used for analysis in this thesis.

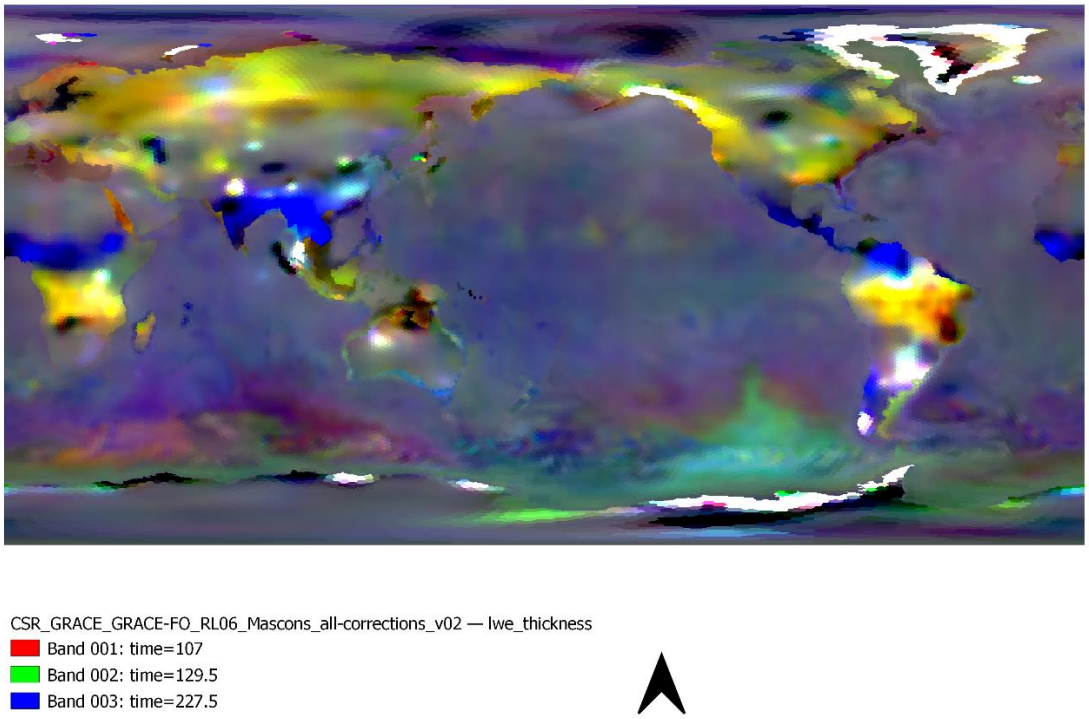

Figure (15) This global map shows several bands of GRACE Terrestrial Water Storage representing monthly timesteps ranging from 2004 to 2021
Source: https://www2.csr.utexas.edu/grace/RL06_mascons.html

3.3.5 Global Land Data Assimilation System (GLDAS)

GLDAS is a modeling and data assimilation framework that provide information on various meteorological and hydrological variables, including precipitation, temperature, soil moisture, and evapotranspiration (NASA, Hualan et al.,2019).

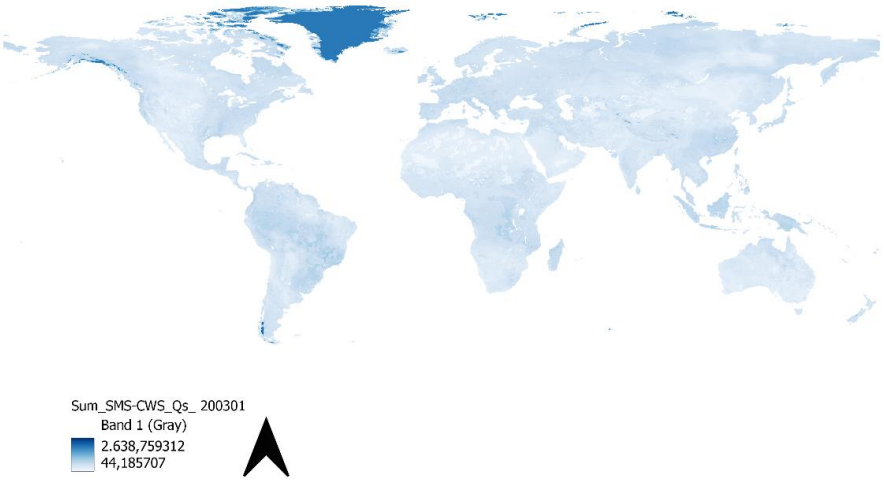

Figure (16) This global map shows one band of GLDAS(SM+CW+Qs) representing one month
Source: https://disc.gsfc.nasa.gov/datasets?keywords=GLDAS.

These datasets are produced using a combination of observational data and numerical models, and are available at different spatial and temporal resolutions. The spatial resolution of GLDAS datasets vary depending on the product and version. The original GLDAS (v1) had a spatial resolution of 0.25 degrees (approximately 28 km) and was updated to 0.5 degrees (approximately 56 km) in the GLDAS-2.0. The newest version of GLDAS (v3) has a spatial resolution of 0.25 degrees. The temporal resolution of GLDAS datasets vary as well, depending on the product and version. The original GLDAS (v1) had a 3-hourly time step, while GLDAS-2.0 and GLDAS-2.1 have a 3-hourly and daily time step, respectively. GLDAS-NOAH 3.0 has a daily time step (NASA, Hualan et al.,2019).

3.3.6 Pre-processing of GRACE and GLDAS for Groundwater Anomaly Analysis

The TWS gotten from GRACE cannot differentiate the different storage compartments, so I acquired all required storage compartments based on my region of interest from GLDAS. For my analysis the components I used includes: Soil Moisture (SM), Canopy Water (CW), and Surface runoff (Qs). Since GRACE cannot differentiate between the different storages and assumes TWS as a combined storage column as seen in figure (17), a likely model was applied to the components gotten from GLDAS, therefore Soil moisture, canopy water and surface runoff were added together: SM + CW + Qs.

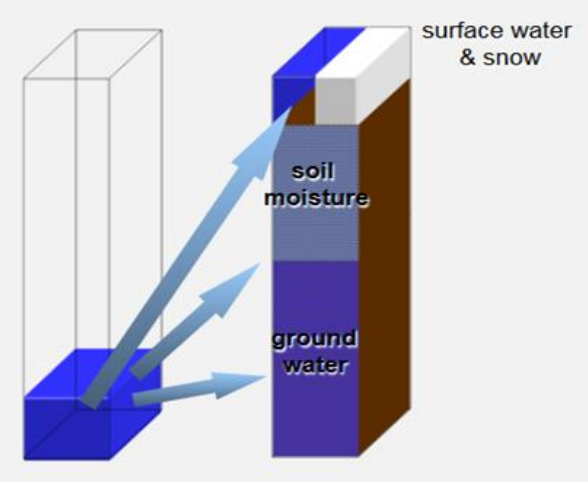

Figure (17) Image showing Vertical or Column TWS
Source: Google Image search

Figure (18) and (19) shows Maiduguri's TWS and SMS+CWS+Qs respectively. As seen in the map just five pixels covers this region due to the poor resolution of GRACE and GLDAS, and for my analysis, I have only considered one pixel because majority of the PS are concentrated in that pixel.

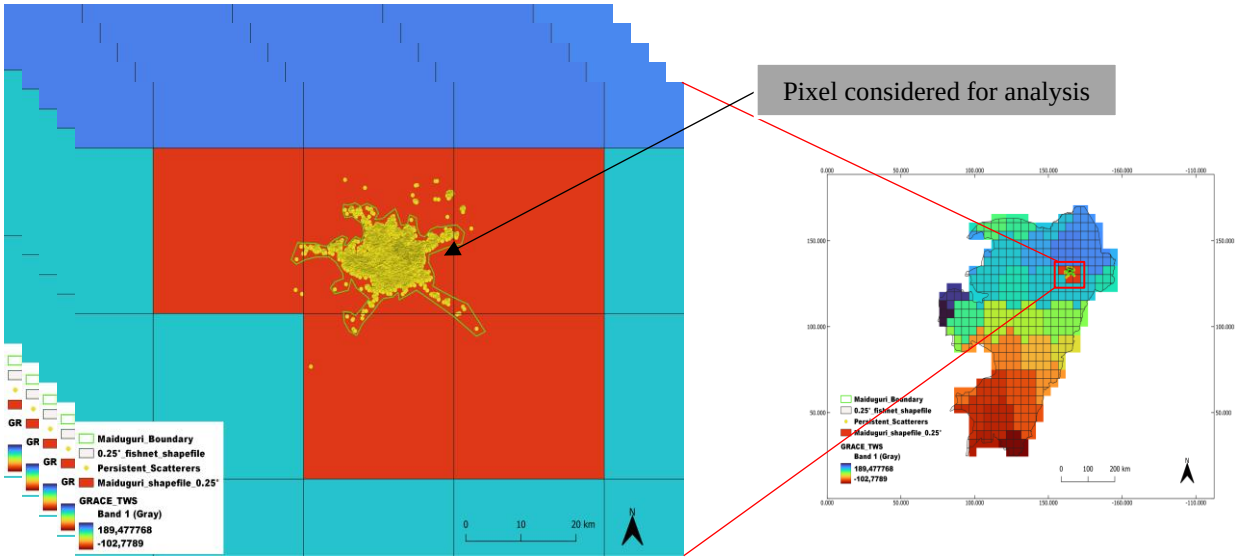

Figure (18) Maiduguri. ΔTWS acquired from GRACE
Source: author

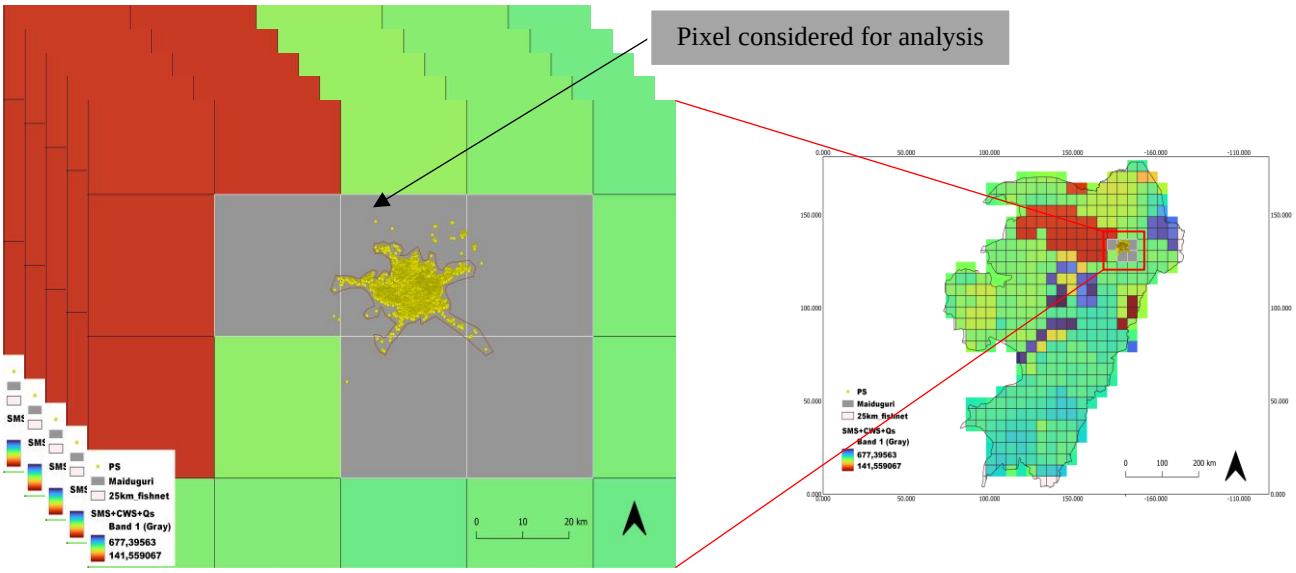

Figure (19) Maiduguri. SMS+CWS+Qs acquired from GLDAS
Source: author

Figure (20) and (21) illustrates the TWS and SMS+CWS+Qs of Marraraba respectively. The map reveals that the entire area is located within a single pixel and indicates that only one-fourth of the pixel is covered by Marraraba's landmass. As a result, my research was conducted on this particular pixel, leading to a biased outcome. However, to ensure the comprehensiveness of my findings, I examined the region's climatology, which is discussed in the later in chapter4.

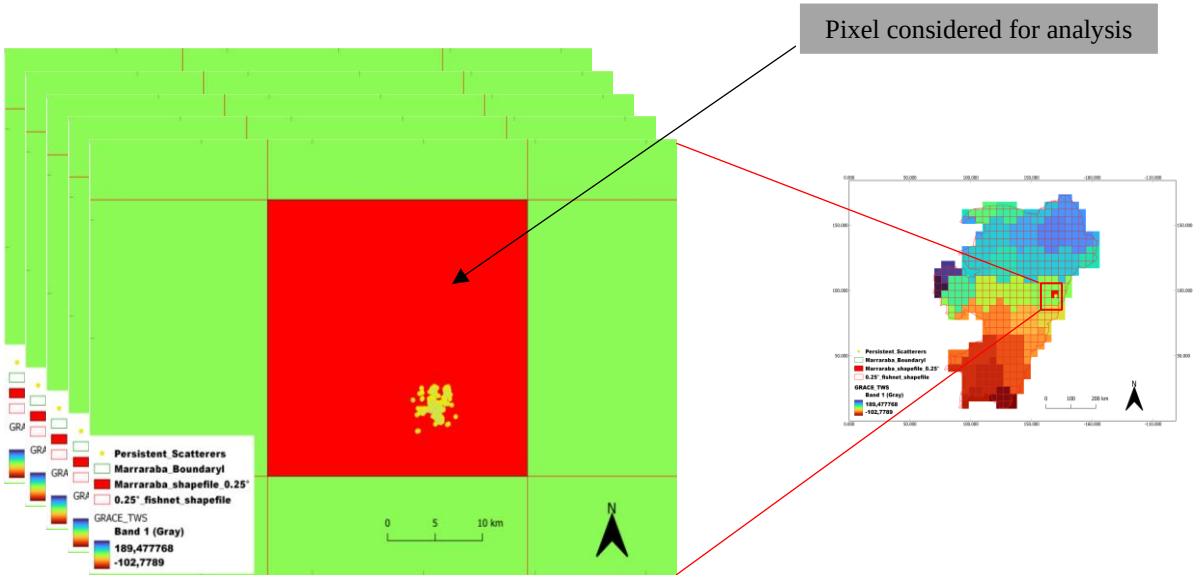

Figure (20) Marraraba. ΔTWS acquired from GRACE
Source: author

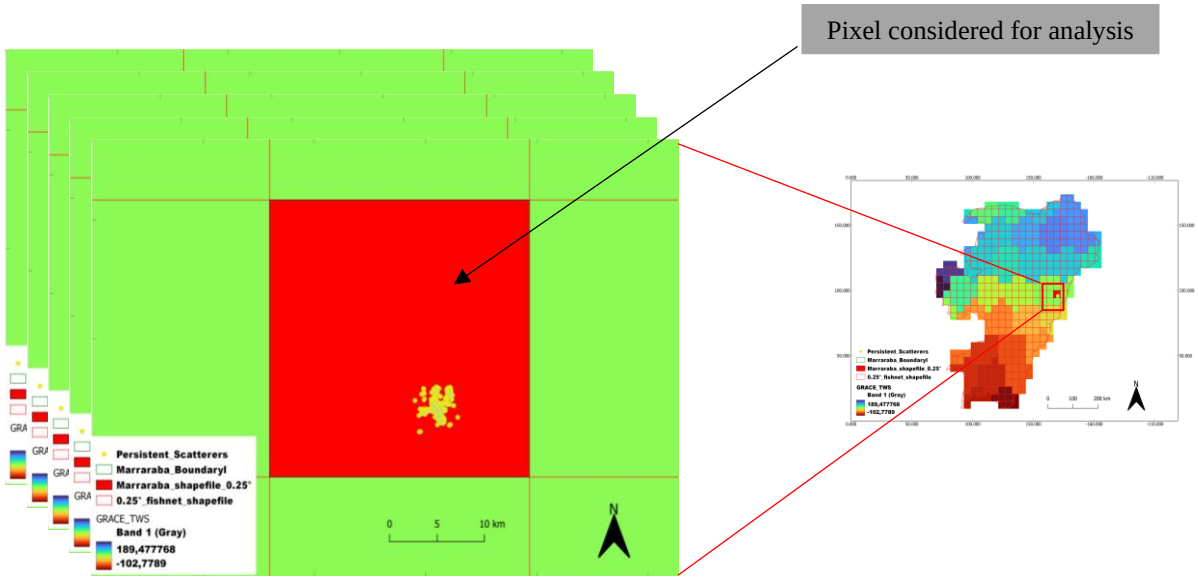

Figure (21) Marraraba. SMS+CWS+Qs acquired from GLDAS
Source: author

The components acquired from GLDAS are not in an anomaly format but they have to be for proper analysis, therefore because an anomaly baseline of 2004-2009 was used for GRACE I have also used an anomaly baseline of 2004-2009 for the components acquired from GLDAS so they can be in the same anomaly format. To derive Groundwater Anomaly using GRACE and GLDAS, the following model was used - $\Delta GWS = \Delta TWS - \Delta(SM+CW+Qs)$.

Below is a flowchart of the process chain line for Groundwater Analysis using GRACE and GLDAS:

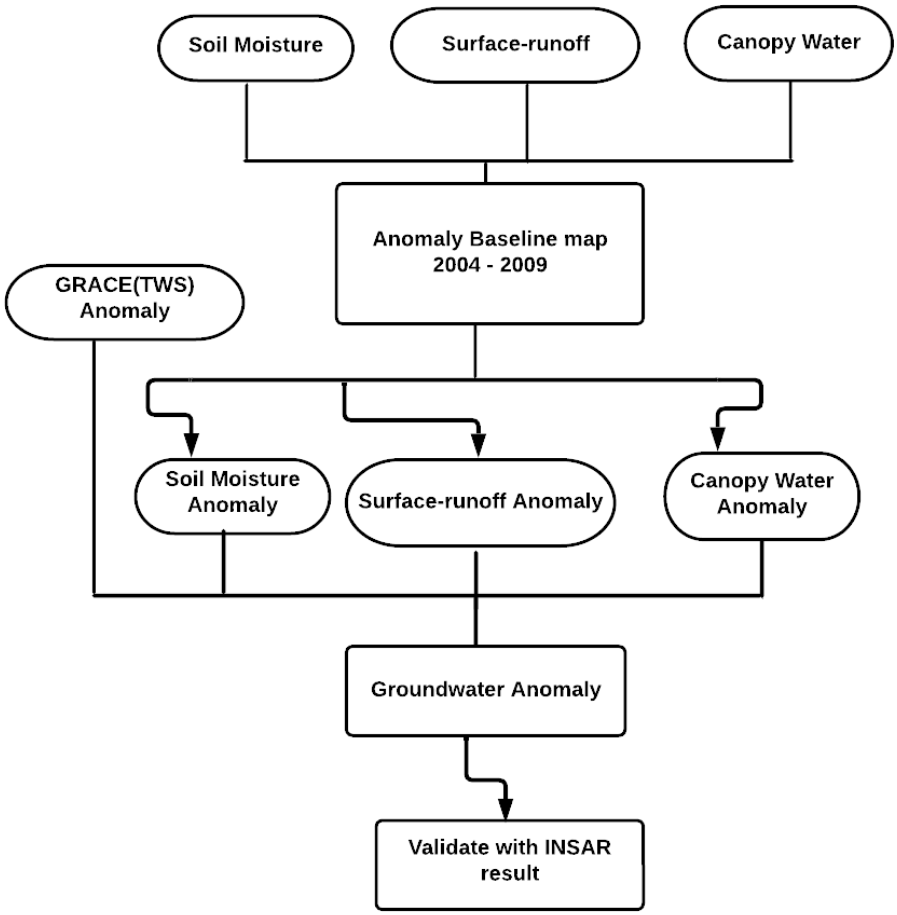

Figure (22) Flowchart-2 for Groundwater anomaly analysis
Source: author

3.3.7 Standardised Precipitation Evapotranspiration Index (SPEI)

SPEI is a drought index that utilizes climate data and considers both precipitation and potential evapotranspiration (PET) to determine the onset, duration, and severity of drought conditions relative to normal conditions. It is applicable to various natural and managed systems, such as crops, ecosystems, rivers, and water resources (Vicente-Serrano et al., 2010). The index incorporates the effects of rising temperatures on water demand and can be computed over timeframes ranging from 1 to 48 months. In this thesis, PET was estimated over a 36-month period using Temperature and Precipitation data, with the **SPEI App** developed by Vicente-Serrano et al. This software is based on the Thornthwaite (1948) method for PET estimation. For a more thorough understanding, please consult the SPEI Manual by Vicente-Serrano et al., 2009.

Figure14(a), (b), (c), and (d), shows the Precipitation and Temperature patterns of Maiduguri and Marraraba respectively. As observed, the precipitation pattern for both regions suggests that June to September experiences the most precipitation through the specified years. It appears that the

temperature patterns for both regions follow a similar trend across the specified years, with January to April showing higher temperatures compared to the other months.

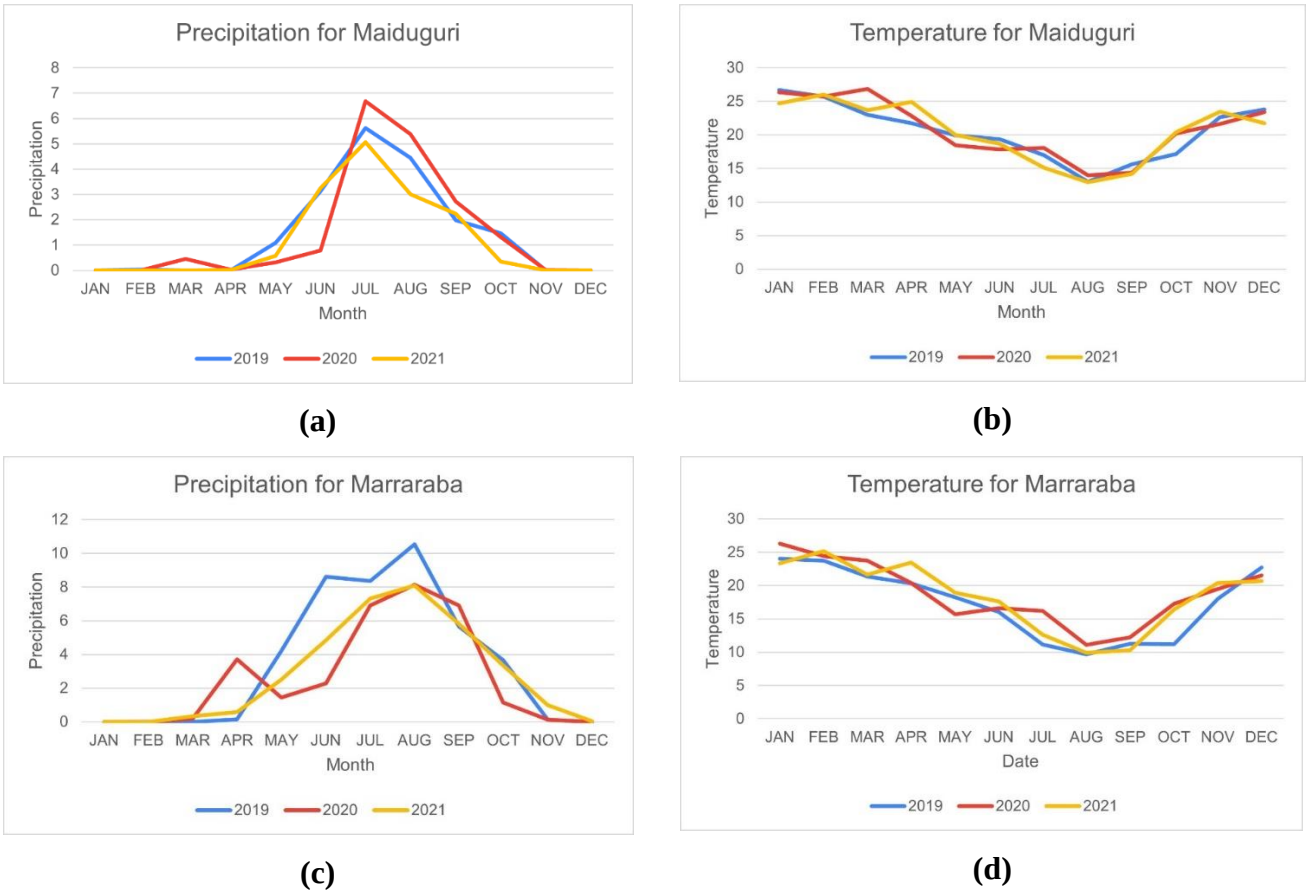

Figure (23) Maiduguri and Marraraba Precipitation (a, c), Maiduguri and Marraraba Temperatures (b, d).

This table contains standard SPEI value ranges used globally to classify SEPI results.

Categories	SPEI Value
Extreme drought	Less than −2.00
Severe drought	−1.99 to −1.50
Moderate drought	−1.49 to −1.00
Near normal	−0.99 to 0.99
Moderately wet	1.00 to 1.49
Severely wet	1.50 to 1.99

Table (3) Showing SPEI value ranges and their meaning

CHAPTER FOUR

4 RESULTS AND DISCUSSIONS

In this chapter, the results of the analysis conducted on Land Deformation, Groundwater Anomaly, and Standardized Precipitation Evapotranspiration Index (SPEI) are presented. The findings are communicated through various approaches, such as observations, representations, translations, and presentations, which collectively offer a comprehensive understanding of the analyzed data.

4.0 Land Deformation Analysis

In order to explore and map the land deformation situation in my areas of interest, I used Sentinel-1 satellite data and applied the methodology described in Chapter 3.

4.0.1 Pre-processing of Sentinel-1 for StaMPS Analysis (Results)

SAR image pre-processing was conducted for both Maiduguri and Marraraba in the SNAP environment. A total of 86 SAR images were processed for Maiduguri and 87 images were processed for Marraraba. To facilitate analysis, the images were stacked together in correspondent to their respective locations. To accomplish this, a master image(figure24a&25a) with an optimal baseline was selected as a reference to calculate phase-shifts from the rest of the images called slaves(figure24b&25b), there results were recorded and interpreted as Interferograms as seen in (figure24c&25c), the colored fringes and the accompanying noise represent the extracted heights of individual points on the ground, with each point being a potential scatterer. As previously mentioned, and elaborated in Chapter 3, the pre-processing of the interferograms involves several steps, which were automated using the Snap2STamPs software package. This was done to ensure that the interferograms were in the correct format and could be properly ingested by the STamPS environment, which is based on MATLAB.

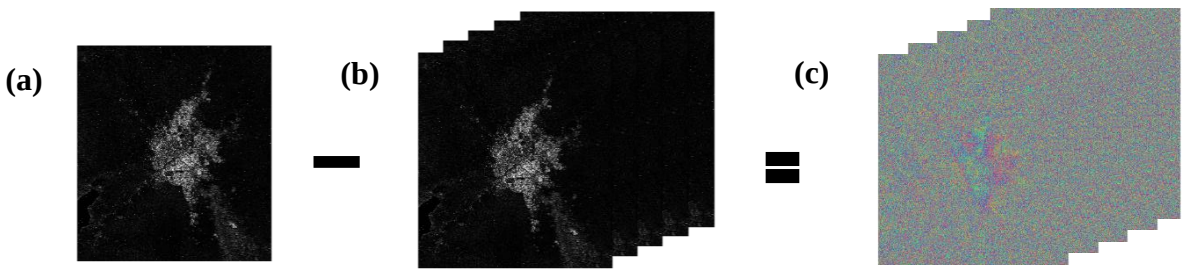

Figure (24) Maiduguri, phase shift generation, where master image(a) is subtracted from individual slave images(b) and recorded as interferograms(c).

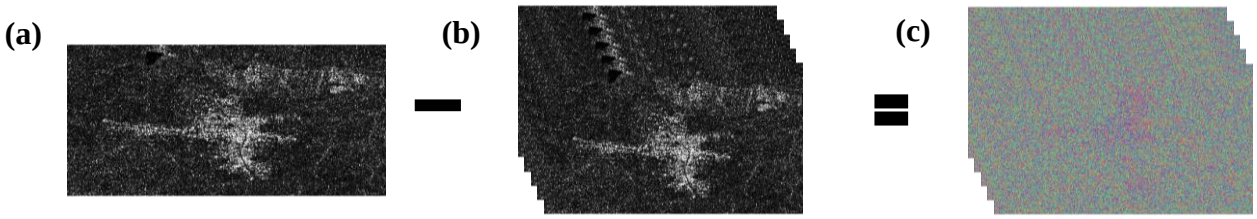

Figure (25) Marraraba, phase shift generation, where master image(a) is subtracted from individual slave images(b) and recorded as interferograms(c).

4.0.2 Implementation of StaMPS

STamPS entail a number of steps as explained in chapter3, after applying the methodology and running steps 1 to 4, the interferograms were processed and shown in figure26((a), (b), (c) and (d)) are 4 randomly selected results of individual interferograms of Maiduguri and Marraraba showing what the Initial selected persistent scatterers look like before weeding and after weeding. After running steps 5, 6, and 7 more noises or errors were eliminated from individual interferograms and reliable persistent scatterers or points were selected.

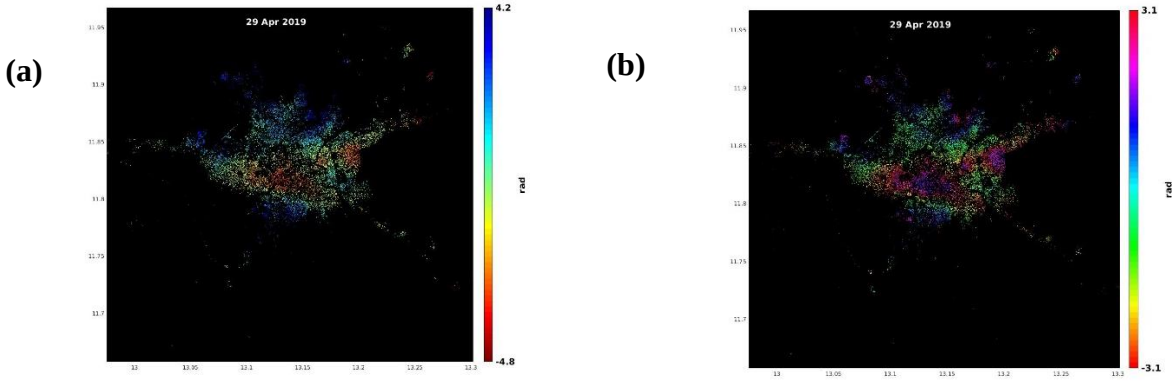

Figure (26) Maiduguri unweeded(a), Marraraba unweeded(b), Maiduguri weeded(a), Marraraba weeded(b)

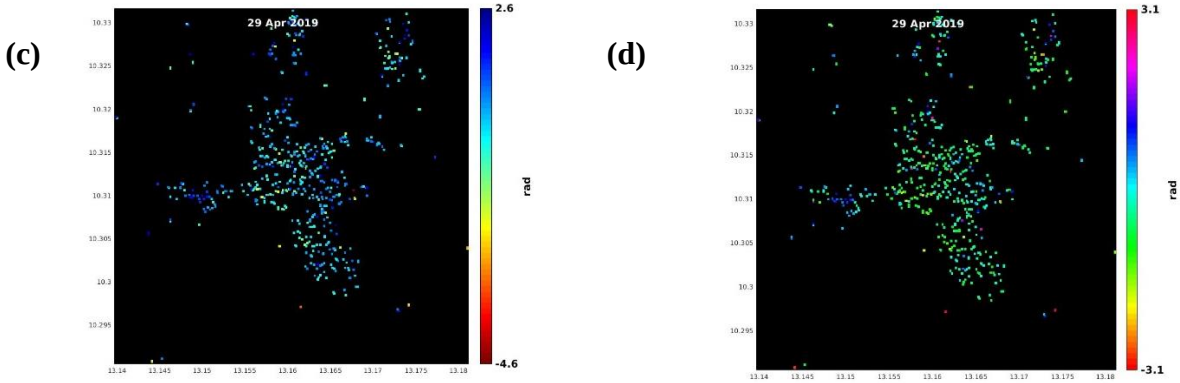

Some of the eliminated errors from both regions are shown in figure (27a, 27d (DEM error), 27b, 27e (Estimated Orbital Ramp error), and 27e,27f (Linear Tropospheric correction error)) respectively.

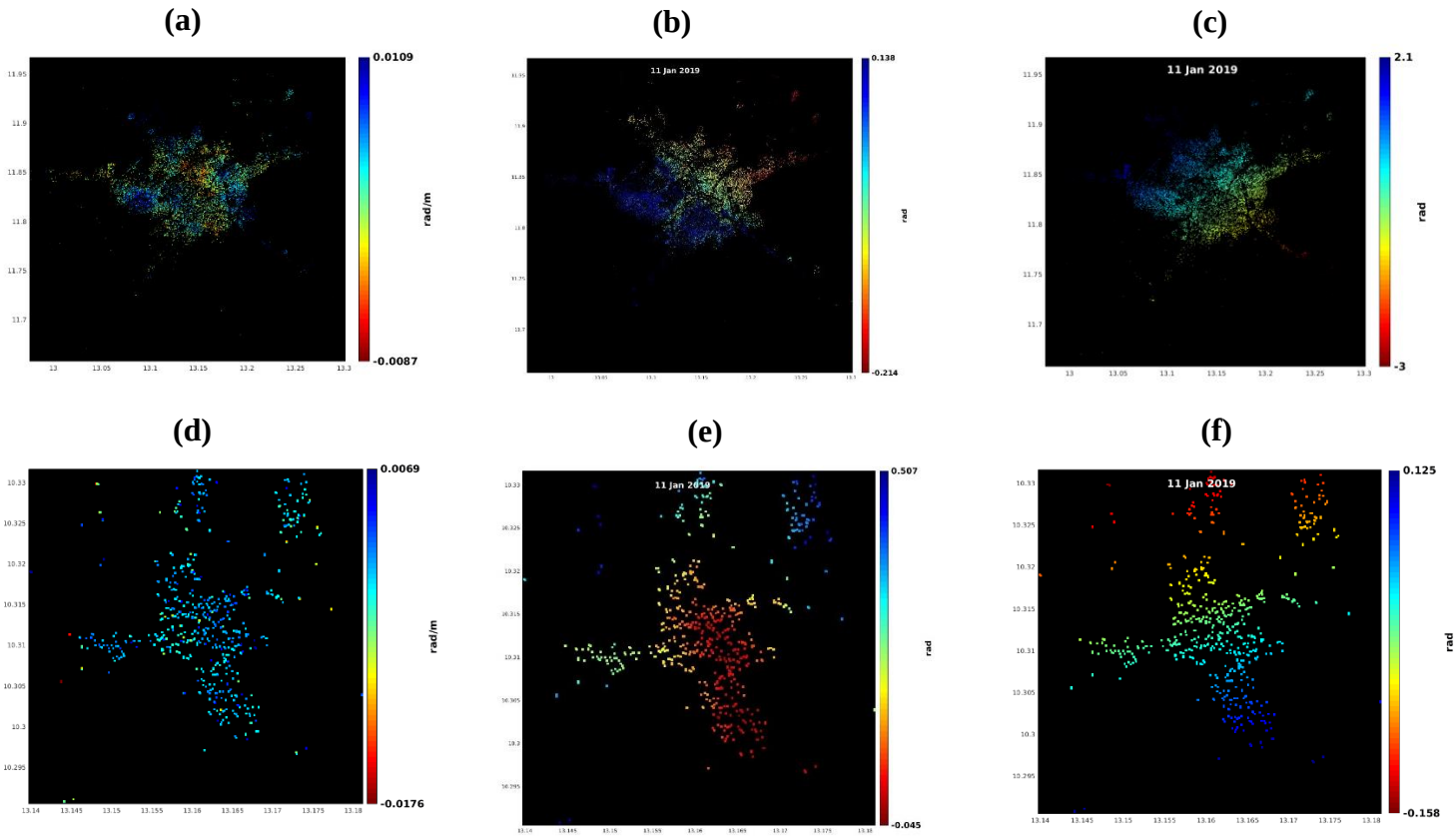

Figure (27). Errors estimated from interferograms for both Maiduguri and Marraraba

4.0.3 Land Deformation Velocity Results for Maiduguri

The mean velocity or land deformation for Maiduguri was estimated after running step 7. The image to the left (figure28a) shows the rate of deformation with positive values signifying uplift and negative values signifying subsidence. Furthermore, this result reveals that the landmass is subsiding as a rate of -6.3mm/year and uplifting at a rate of 6.4mm/year variably.

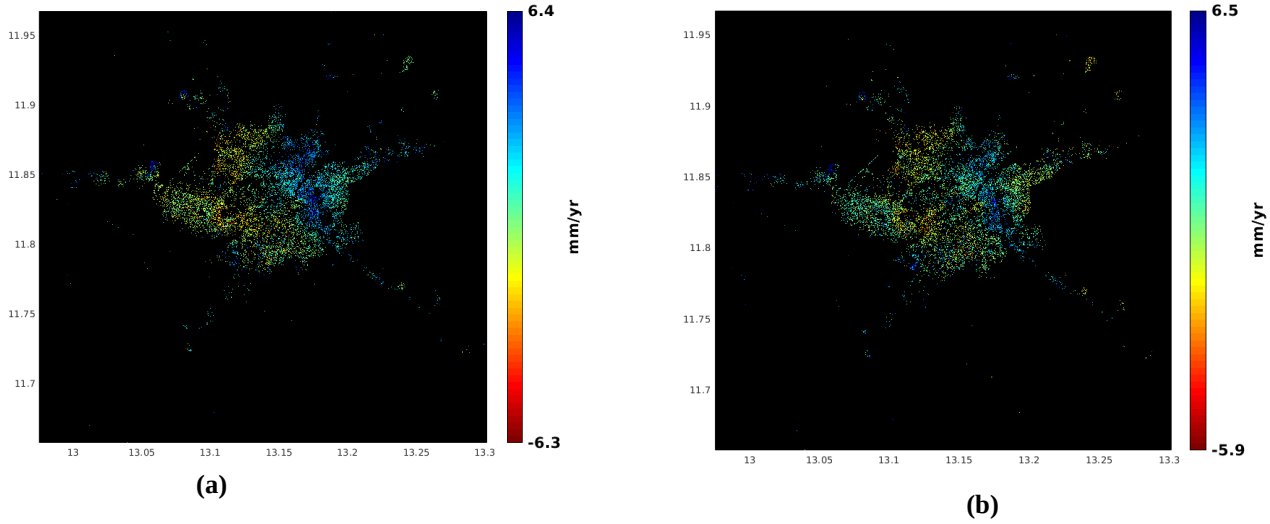

Figure (28) Maiduguri. Estimated Mean Velocity(a) and Estimated Mean Velocity minus

In figure (28), the rate of deformation represented in (a) has inherently eliminated some errors while running the STamPS steps, but some other errors that were generated apart also needs to be subtracted from (a), so the image on the right (figure28b) shows the result of subtracting the remaining errors from the estimated mean velocity. The individual errors used are; DEM estimated error, estimated orbital ramp and tropospheric correction.

Figure (29) below shows the cumulative PS over Maiduguri region as seen in (b), the average of the PS (a) was calculated and the graph (c) shows a temporal deformation pattern of the entire landmass.

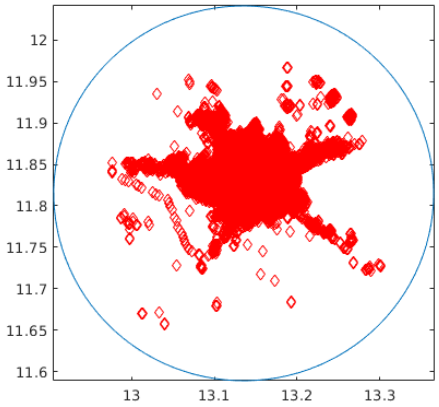

(a)

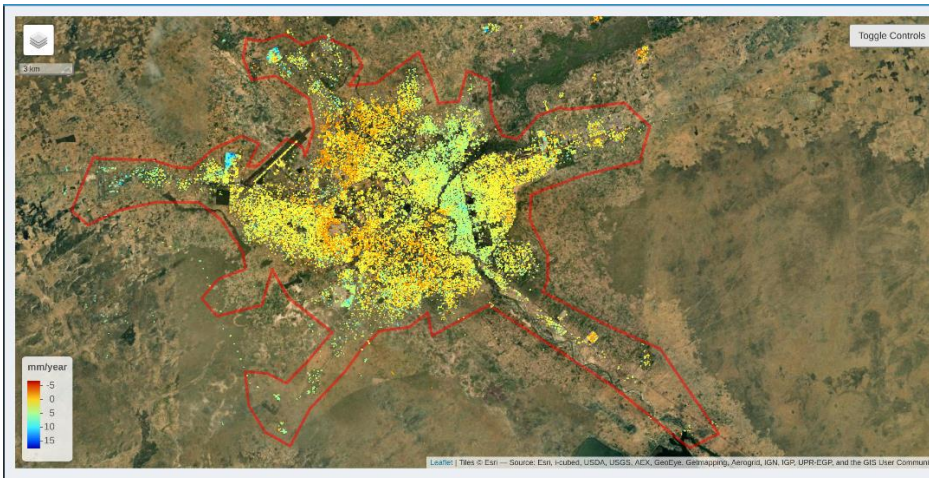

(b)

Figure (29a & b). Maiduguri. Estimated cumulative PS

Based on the results, the linear pattern of deformation shows a gradual uplift through the specified years. however, the temporal pattern shows evidences of subsidence especially in the first half and towards the end of 2019. A consistent gradual uplift is also observed in the first half of 2021.

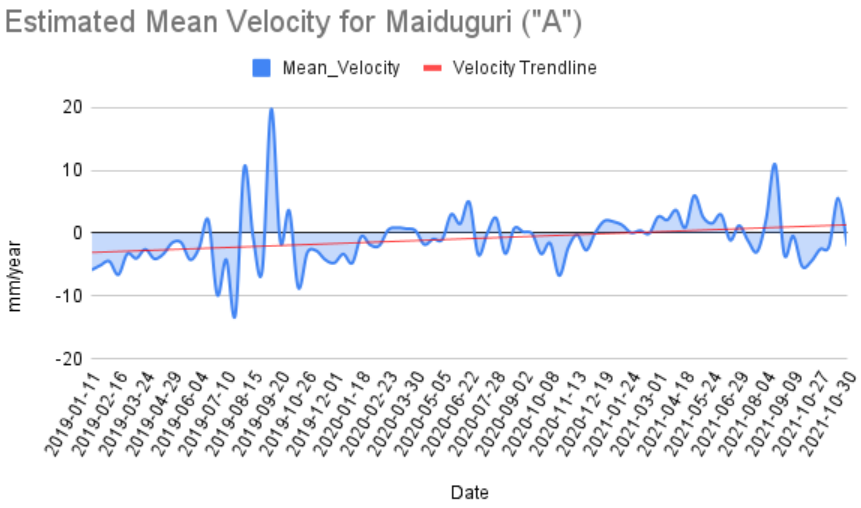

Figure (30). Maiduguri. Estimated Mean Velocity Line Of Sight (LOS)

These variations in ground movement observed in Maiduguri are pointers to an occurrence, but not necessarily conclusive evidence of changes in groundwater levels over the specified years. As

explained in chapter1, a few factors could be responsible for the occurrence of Land Deformation in a particular region, which can also be influenced by the natural characteristics of that location. Nevertheless, this is by far a complex phenomenon as it involves an interplay between natural and human influences. The natural construct of Maiduguri Nigeria suggests that groundwater variation could be a major cause of land deformation since occurrences such as earthquake or tectonic shifts do not occur in this region and in Nigeria as a whole.

To have a better understanding of these variations, I observed the scatterers at two different areas in Maiduguri with a 100m radius as seen in figure (31).

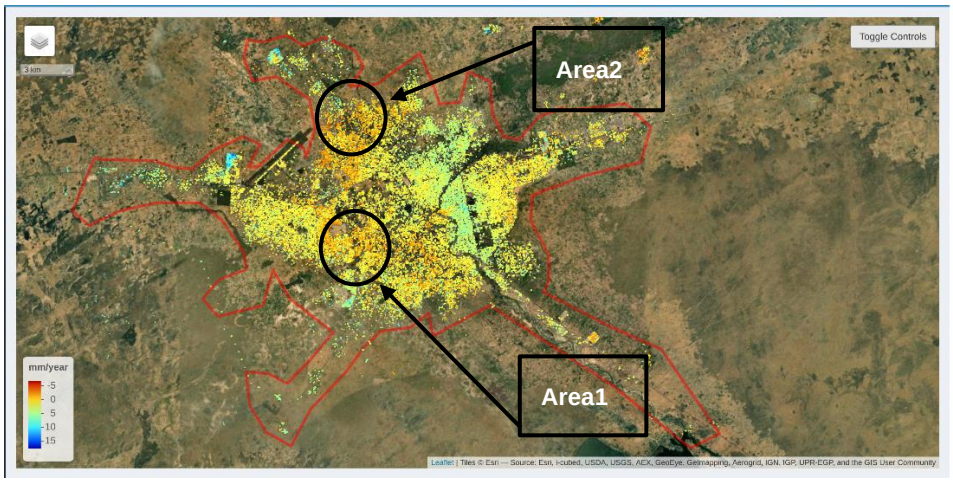

Figure (31) Maiduguri. A Closer observation of Area-1 and Area-2

Figure (32&33) shows the selected PS at Area-1 and Area-2, also represented is the temporal land deformation pattern as presented in the graphs on the left for both areas respectively. The linear temporal patterns for these two areas as seen in Figure (32) and (33) suggests that the land is in fact subsiding. This could mean that groundwater is depleting in this part of Maiduguri, this however have to be verified accordingly.

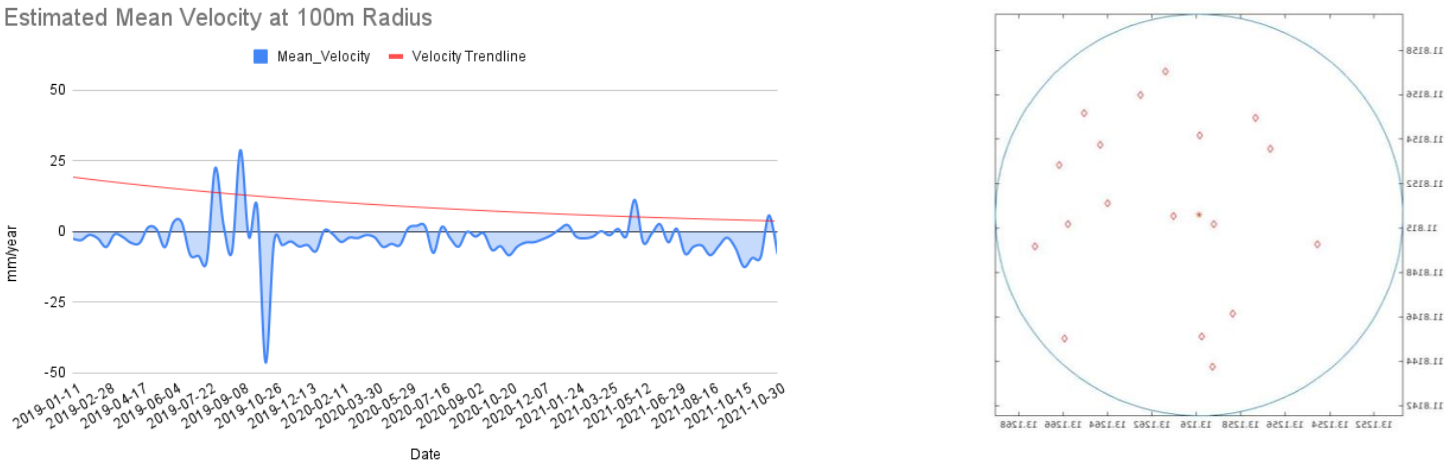

(a) **(b)**

Figure (32) Maiduguri Area-1. Estimated Mean Velocity(a) and PS points selected at a radius of 100m(b).

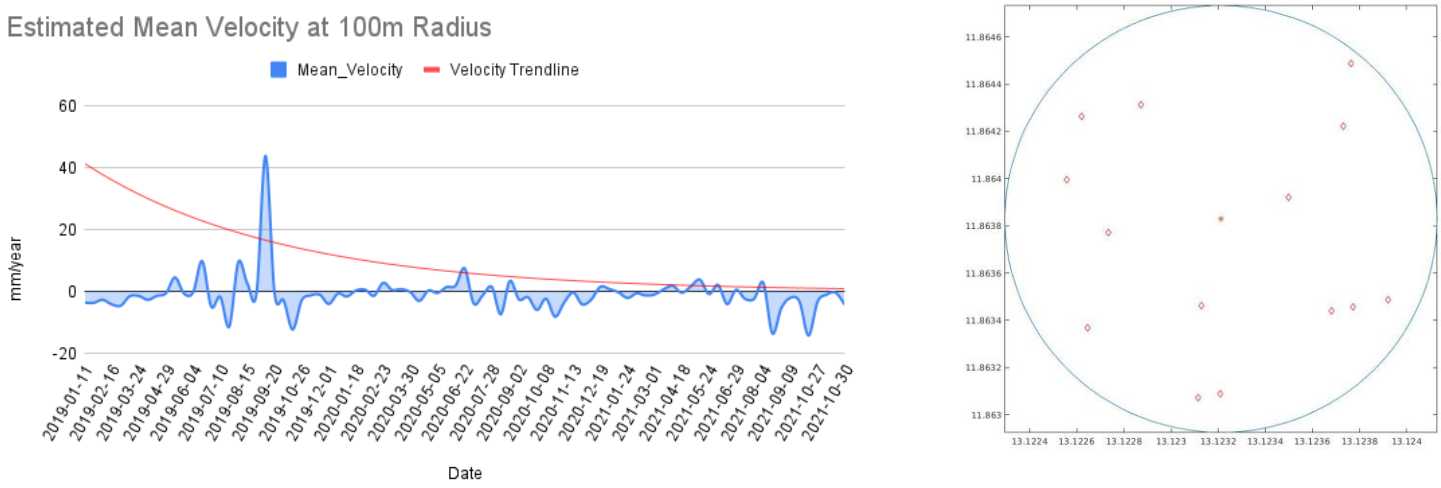

(a) **(b)**

Figure (33) Maiduguri Area-2. Estimated Mean Velocity(a) and PS points selected at a radius of 100m(b).

4.0.4 Land Deformation Velocity Results for Marraraba

Upon running step 7, the average velocity or land deformation for Marraraba was determined. The deformation rate is displayed in Figure (34a), where positive values indicate uplift and negative values indicate subsidence. Although this image has eliminated some errors generated during the STamPS steps, other errors were also generated that need to be removed from (figure34a). Figure (34b) shows the output after subtracting the remaining errors from the estimated mean velocity. As observed the landmass seem to be subsiding at a rate of -5mm/year and uplifting at a rate of 3.2mm/year.

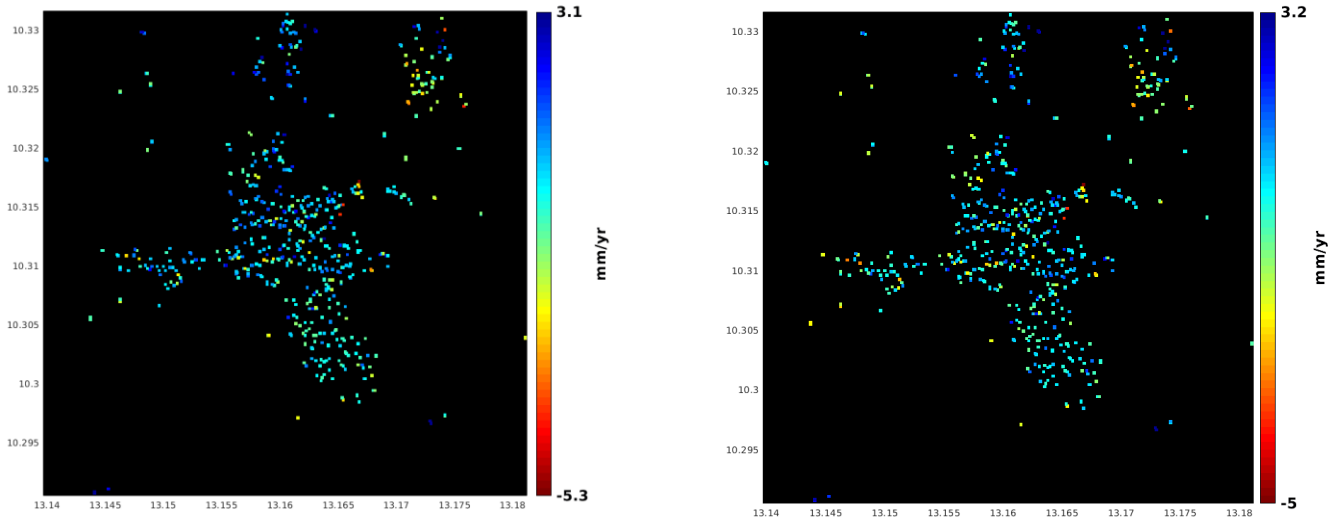

(a) **(b)**

Figure (34) Marraraba. Estimated Mean Velocity(a) and Estimated Mean Velocity minus

Similar to Maiduguri, the individual errors taken into account for Marraraba include the estimated error of the DEM, the estimated orbital ramp, and the tropospheric correction.

The cumulative PS over Marraraba region is illustrated in Figure 35, with (b) displaying the overall distribution and (a) depicting the PS to be averaged.

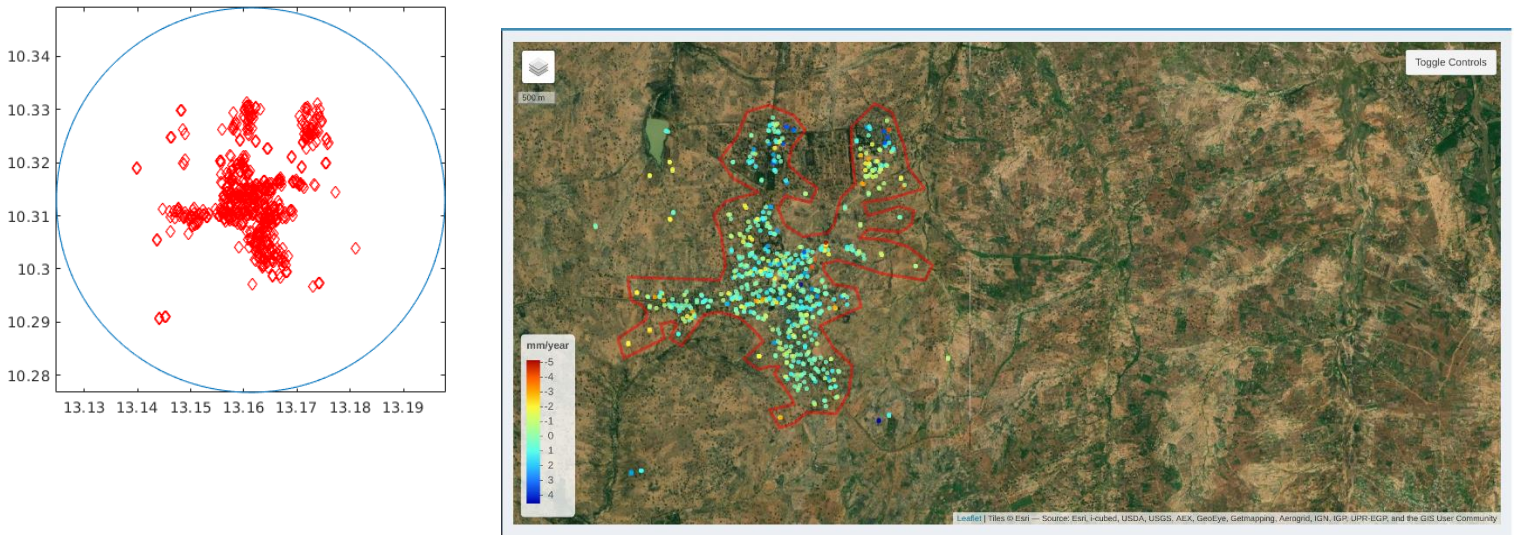

(a) **(b)**

Figure (35) Marraraba. Estimated cumulative PS

The findings indicate that the linear deformation pattern for Marraraba displays a subtle uplift over the specified time period. However, the temporal pattern demonstrates a few subsidence trends, particularly at the first quarter of 2019, June and July of 2020 and mid of 2021. In addition, there seem to be a lot of uplift observed through the specified years.

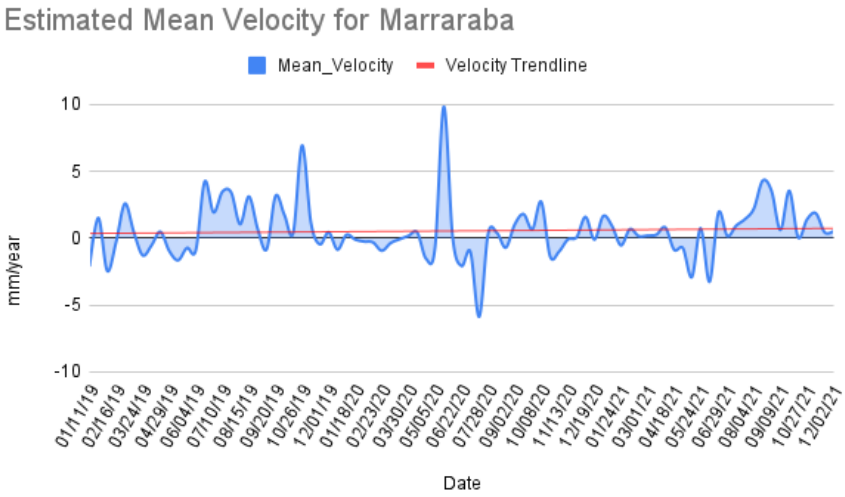

Figure (36) Marraraba. Estimated Mean Velocity Line Of Sight

The fluctuations in ground movement detected in Marraraba suggest that an event is taking place, although they do not necessarily provide conclusive evidence of changes in groundwater levels over the specified years. However, the natural characteristics of Marraraba, which are similar to those of Maiduguri, indicate that groundwater variation may be a significant contributing factor to land deformation since phenomena such as earthquakes or tectonic shifts do not typically occur in this region or in Nigeria as a whole.

Similar to Maiduguri, in order to gain a better understanding of these variations, two different areas in Marraraba were observed by analyzing the scatterers within a 100m radius. This can be seen in Figure 37.

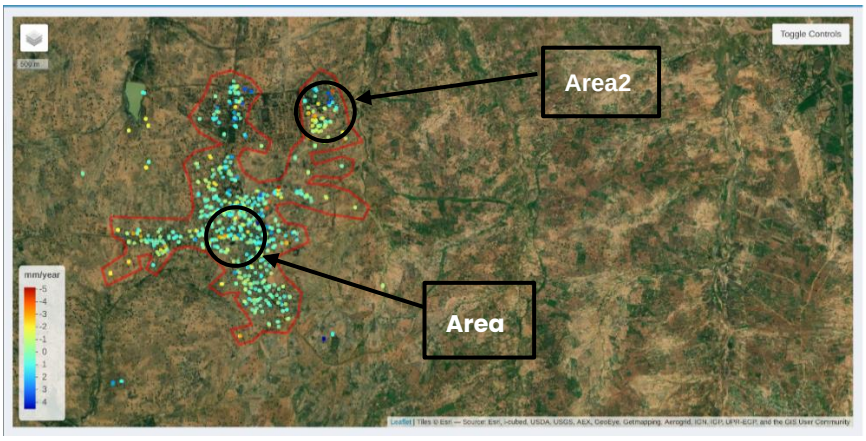

Figure (37) Marraraba. A Closer observation of Area-1 and Area-2

Figure 38 and 39 displays the chosen PS located in Area-1 and Area-2 respectively, and the figure also presents the temporal land deformation pattern depicted on the left-sided graphs for both areas,

respectively. The observed linear pattern in these graphs indicates that the land is subsiding in both areas. This finding raises the possibility that the groundwater in this specific part of Marraraba may be decreasing or depleting. However, further verification is needed to confirm this hypothesis.

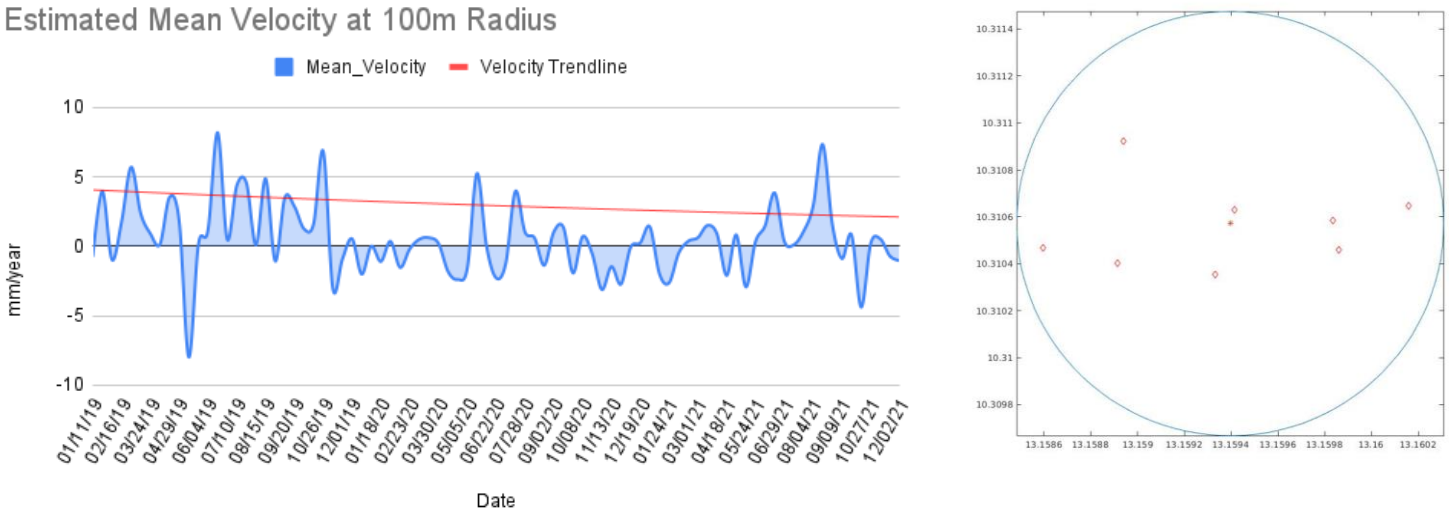

Figure (38) Marraraba Area-1. Estimated Mean Velocity(a) and PS points selected at a radius

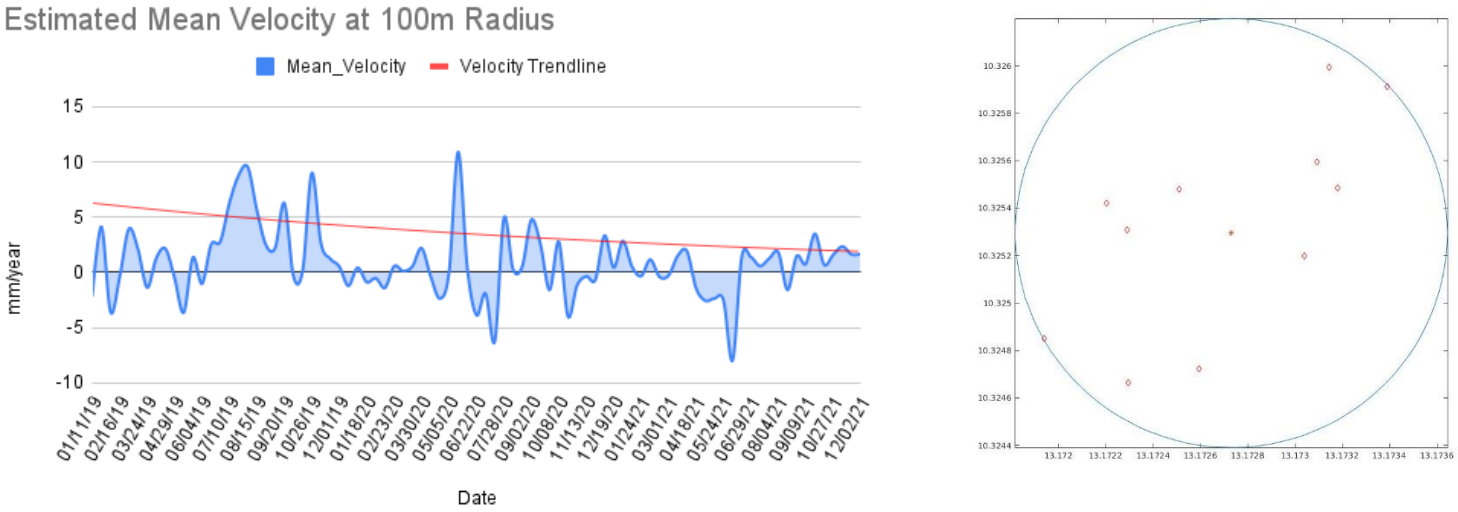

(b)

Figure (39) Marraraba Area-2. Estimated Mean Velocity(a) and PS points selected at a radius

4.1 Groundwater Anomaly Analysis

Although land deformation can provide valuable information about changes in the land surface, it does not necessarily explain why the land is sinking or rising. This could be due to a few factors such as tectonic shifts, groundwater depletion or recharge. Therefore, in addition to analyzing land

deformation, I have also analyzed Groundwater Anomaly using Terrestrial Water Storage (TWS) data obtained from the GRACE satellite missions and GLDAS modeling and data assimilation framework to estimate Groundwater anomaly so as to support my findings.

4.1.0 Groundwater Anomaly Estimation Results for Maiduguri

To calculate the groundwater anomaly for Maiduguri, it is necessary to have all datasets in an anomaly format. While TWS is already in this format with an anomaly baseline of 2004 to 2009, data from GLDAS are not and must be transformed to match TWS. As detailed in chapter 3, an anomaly baseline of 2004 to 2009 was also applied to derive the anomalies for the specific years of interest (2019-2021). Figure 14 and 15 shows the temporal patterns of TWS and SW+CW+Qs respectively.

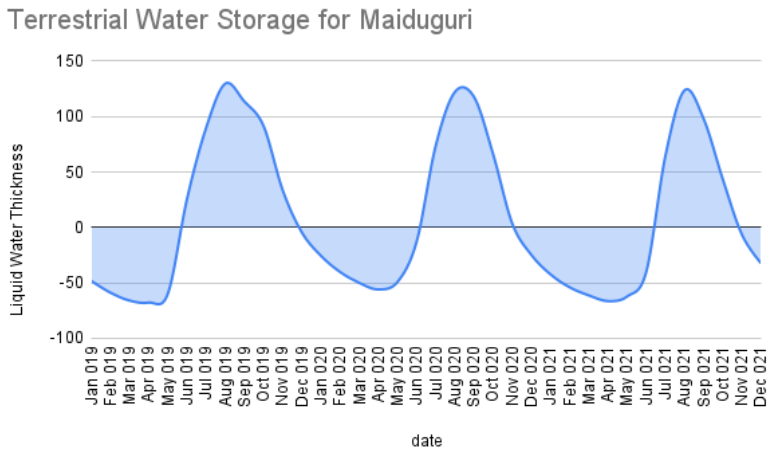

Figure (40) Maiduguri. **Δ**TWS acquired from GRACE

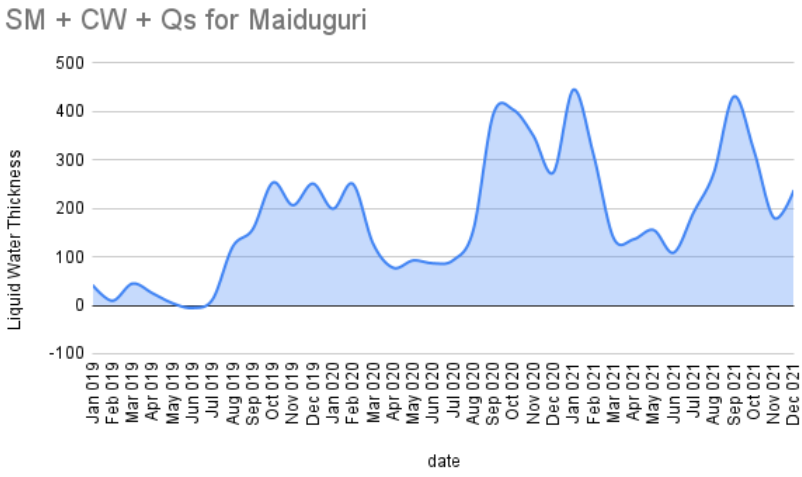

Figure (41) Maiduguri. **Δ(**SMS+CWS+Qs) acquired from GLDAS

Once all my data are in an anomaly format, I implemented the method below to estimate Groundwater Anomaly for the specified years.

ΔGWS =ΔTWS – Δ(SM+CW+Qs)

- ***SM*** *– Soil Moisture*
- ***CW*** *– Canopy Water*
- ***Qs*** *– Surface Runoff*
- ***ΔTWS*** *– Change in Terrestrial Water Storage*
- ***ΔGWS*** *– Change in Groundwater Storage*

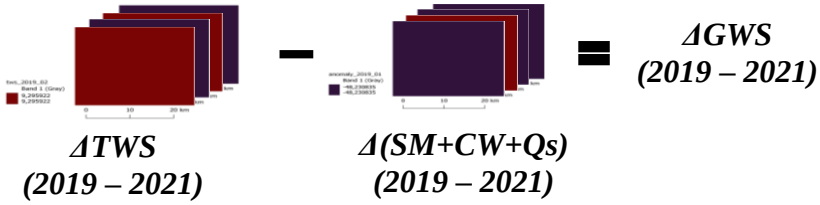

Figure (42). Illustration of analysis

According to the findings, the GW anomaly in Maiduguri indicates the existence of groundwater through a linear trend. Nevertheless, a noticeable decline is observed in July of each year, with 2019 recording the most water level fall, while the water level peaked at the start of 2021 and steadily declined and increased until the close of the year.

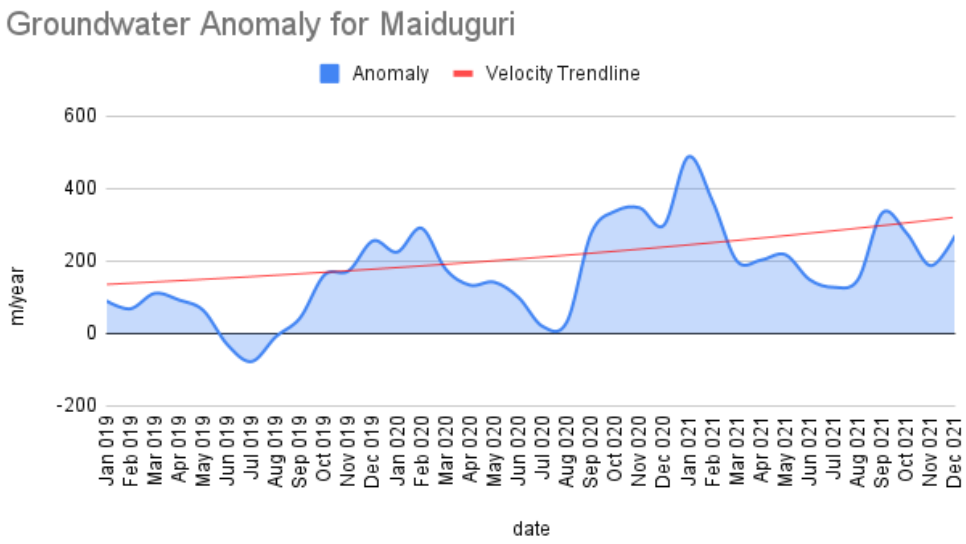

Figure (43) Maiduguri Estimated Groundwater Anomaly

4.1.1 Groundwater Anomaly Estimation Results for Marraraba

To obtain the groundwater anomaly for Marraraba, all datasets must be converted into an anomaly format just as it was done for Maiduguri. The temporal patterns of TWS and SW+CW+Qs are presented in Figure 14 and 15, respectively.

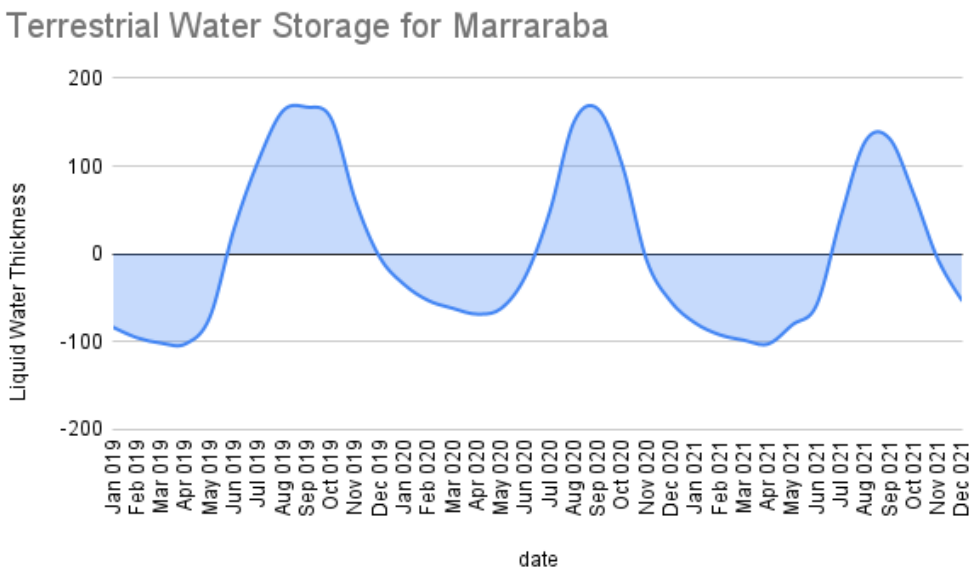

Figure (44) Marraraba. ΔTWS acquired from GRACE

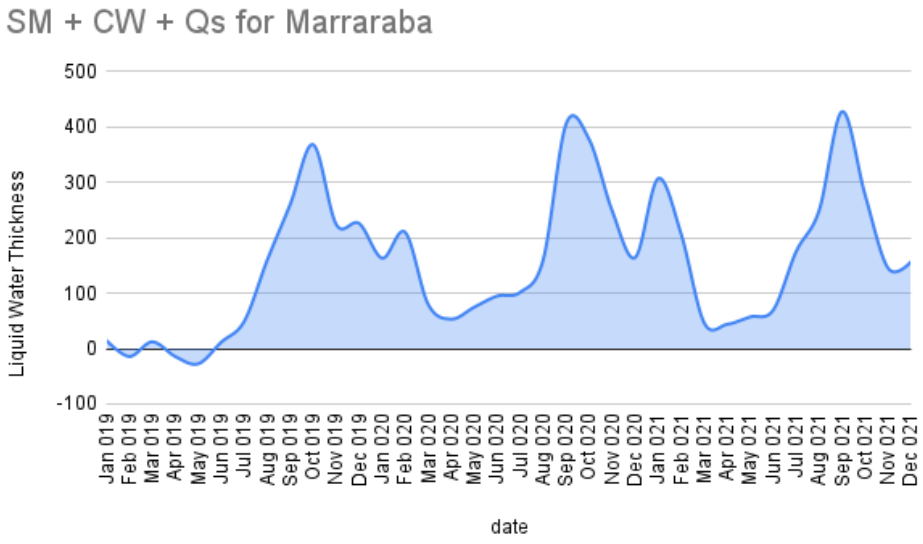

Figure (45) Marraraba. **Δ(**SMS+CWS+Qs) acquired from GLDAS

The research findings reveal that the groundwater anomaly in Marraraba exhibits a linear trend, indicating the presence of groundwater. However, a significant decrease is noticeable in July of 2020 and with 2019 experiencing the most pronounced drop in water levels. The water levels reached their peak at the beginning of 2021, but then gradually declined and rose in September of the same year.

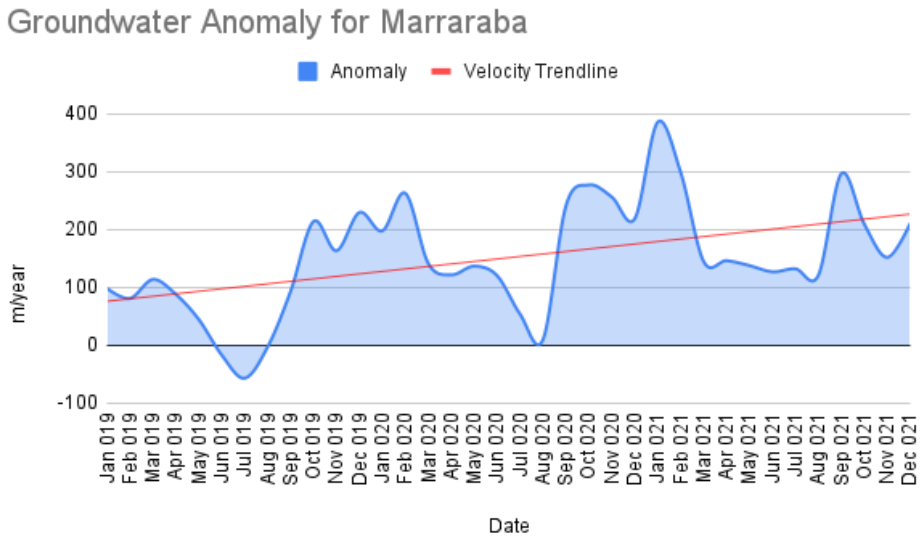

Figure (46) Marraraba. Estimated Groundwater Anomaly

4.2 Comparison Validation of Groundwater Anomaly and Land Deformation

To support the claims from my findings I observed the temporal trend of Land Deformation and Groundwater Anomaly realized from my analysis.

4.2.0 Comparison Validation for Maiduguri

The following image depicts a temporal comparison between the land deformation and groundwater anomaly outcomes from the analysis. As indicated in the graph, the linear trends of both results imply the existence of groundwater. Additionally, there are some notable similarities in drops and rises over the specified years.

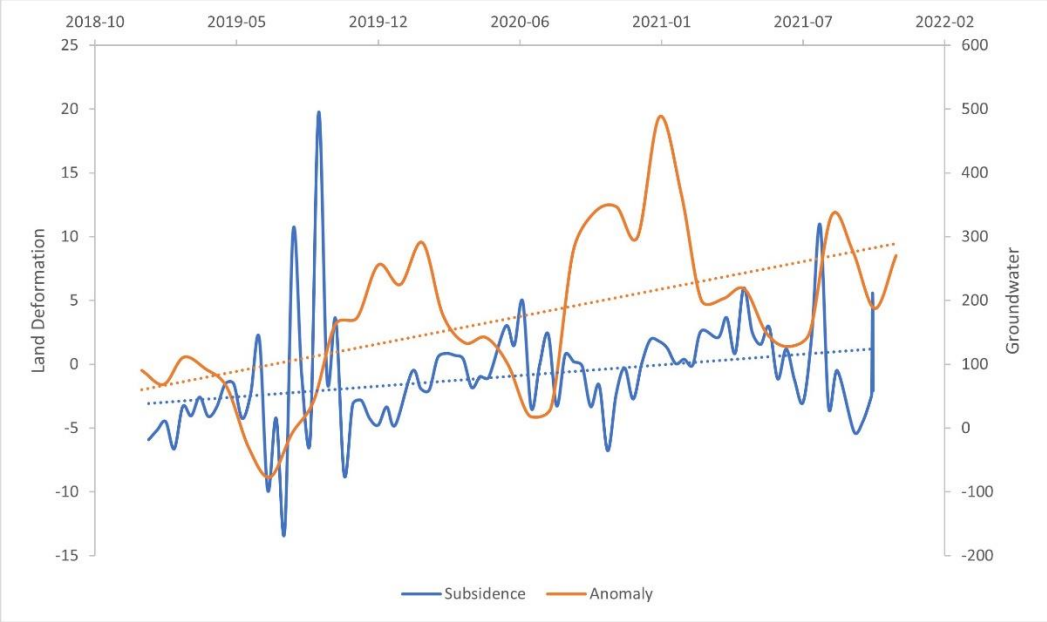

Figure (47) Maiduguri. Groundwater Anomaly and Ground deformation validation

Upon observation, there appears to be a similar drop trend in both land deformation and groundwater anomaly results during the first quarter of 2019. Additionally, a similar rise trend is observed in both results at the beginning of 2020. It is also worth noting the sudden increase in both results towards the end of 2021.

4.2.1 Comparison Validation for Marraraba

Figure. 19 presents a comparison of the temporal patterns demonstrated by the results obtained from the analysis of both land deformation and groundwater anomaly for Marraraba. The individual linear trends for both groundwater and land deformation indicate a rise over the specified years. However, the groundwater trend appears to be more pronounced than the land deformation trend. This could be due to differences in resolution, as the landmass of Marraraba only covers one-fourth of the pixel from GRACE, as depicted in the map in Figure 26.

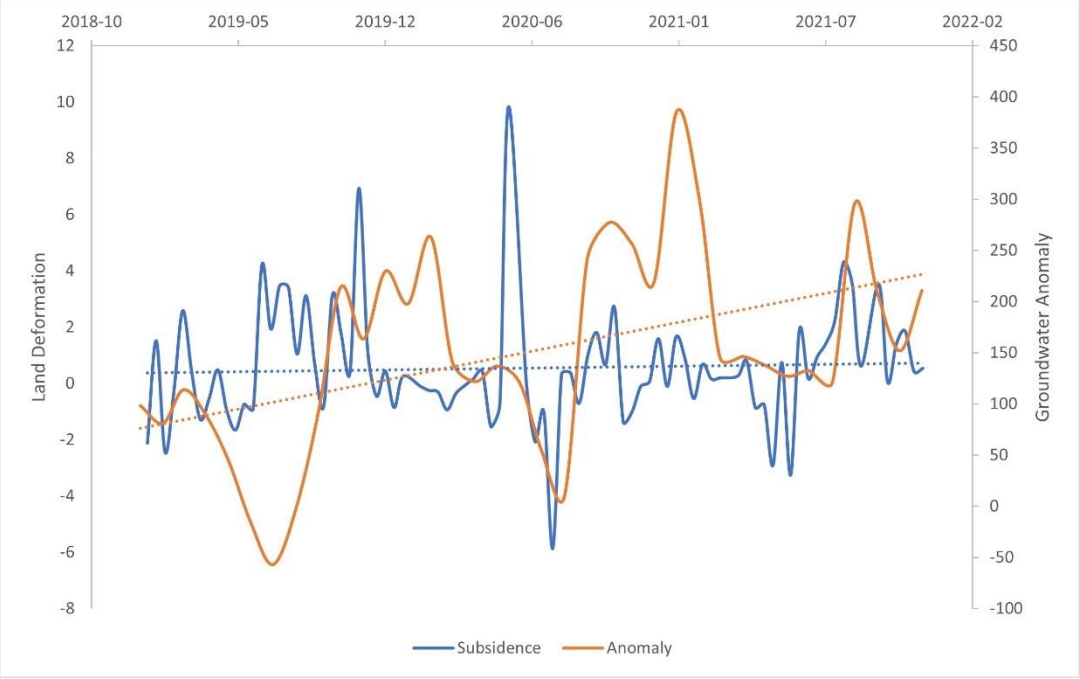

Figure (48) Marraraba Groundwater Anomaly and Land deformation validation

Upon examining the results, there appears to be a similarity in the drop observed in both groundwater and land deformation results during July of 2020. Furthermore, towards the end of 2020 and the beginning of 2021, the trends of both results seem to be moving in a similar direction. Finally, the end of 2021 displays a comparable trend for both outcomes. Due to the biases in these results, which is as a result of differences in resolution and the lack of in-situ data, I have done some further validations with the results I realized from SPEI.

4.3 Further Comparison Validations with SPEI

For further validations, I considered the Temperature and Precipitation indices and examined their patterns in relation to Maiduguri and Marraraba. This enabled me to understand the drought condition in these regions by calculating the SPEI which has been explained in chapter3.

4.3.0 SPEI Estimation Results for Maiduguri

Figure1 shows the evolution of the SPEI for the specified time scale of 2019 to 2021. As observed, the longest and most severe droughts were recorded in September 2019 and February 2021 with an SPEI approximate value of -1.9 and -1.6 respectively, this falls in the category of severe drought as explained in table2**.** Furthermore in 2021, the drought series show a high frequency of drought and most periods of short drought duration. Also, the drought occurrence in 2019 show a low frequency compared to 2020 and 2021. The drought seems to have an incremental temporal progression through the specified years.

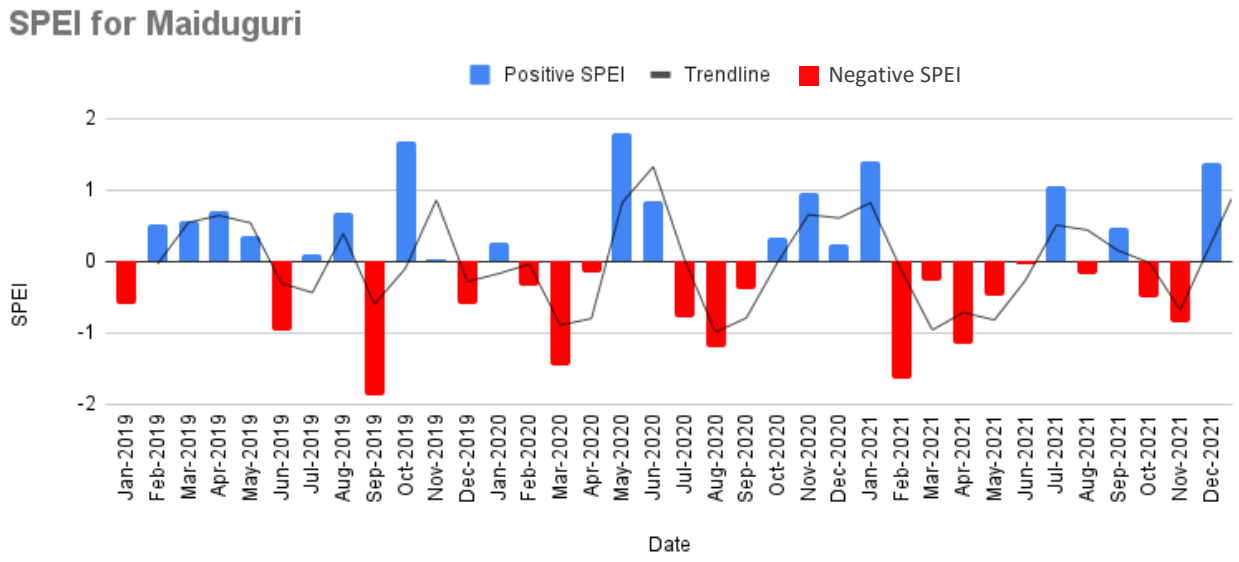

Figure (49) Estimated SPEI for Maiduguri

4.3.1 Comparison Validation for Maiduguri using SPEI and Groundwater Anomaly Results

Figure20 below shows a similar trend between Groundwater Anomaly and SPEI, as observed, in the beginning of 2020 there seem to be a rise in Land deformation and SPEI and a notable drop is observed in 2022. Another notable temporal trend is observed at the end of 2020 into 2021, these variations and trend movement suggests that there is a high possibility that groundwater is depleting and recharging.

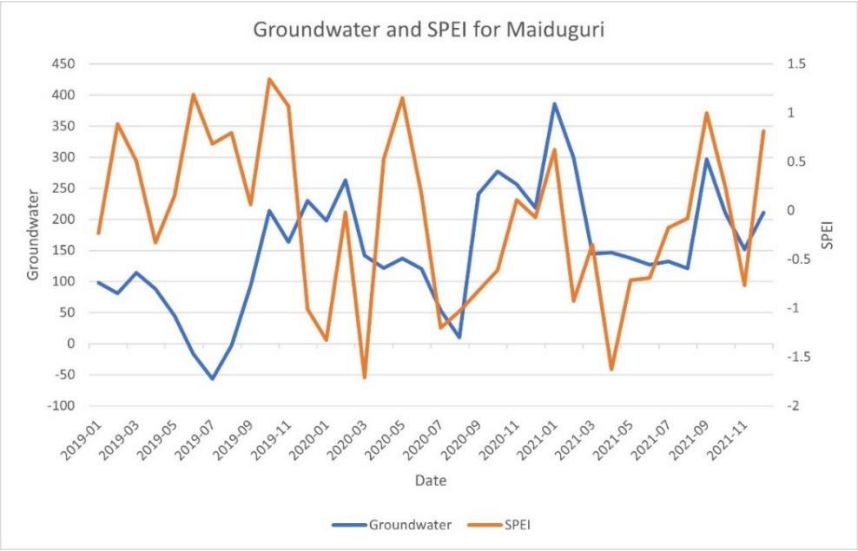

Figure (50) Maiduguri. Groundwater Anomaly and SPEI

4.3.2 Comparison Validation for Maiduguri Area1 using SPEI and Land Deformation Results

Figure51 below shows that a similar trend exists between Land Deformation and SPEI, as observed, 2019 records rise as high as1.6 for SPEI and Land deformation as low as -40 which suggests that

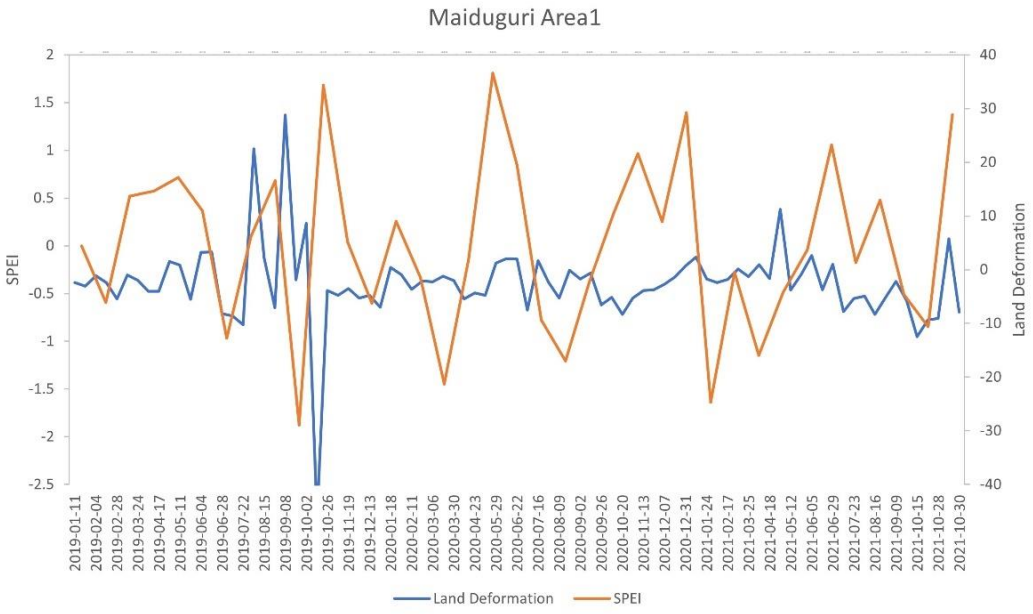

Figure (51) Maiduguri Area1. Land deformation and SPEI

Groundwater is depleting and rising. Similarities in trends are also observed in 2019 and 2021.

4.3.3 Comparison Validation for Maiduguri Area2 using SPEI and Land Deformation Results

Figure52 below shows a temporal variation comparison between Land Deformation and SPEI. As observed, there seem to be a similarity of drops in both trends in 2019 and 2021. Also notable are the subtle rises and drops through the specified years.

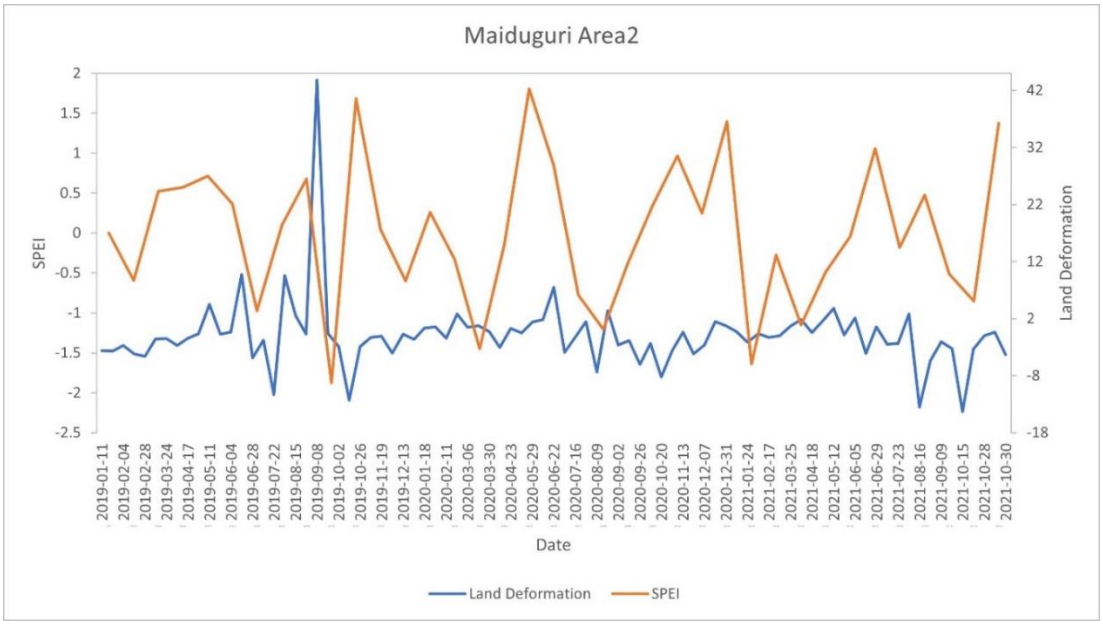

Figure (52) Maiduguri Area2. Land deformation and SPEI

4.3.4 SPEI Estimation Results for Marraraba

The Standardized Precipitation Evapotranspiration Index (SPEI) for the specified time frame of 2019 to 2021 is illustrated in Figure 1. The graph suggests that the most drought periods occurred in February 2020 and March 2021, with an approximate SPEI value of -0.02 and -0.3 respectively, both of which fall into the near normal category, as shown in Table 2.

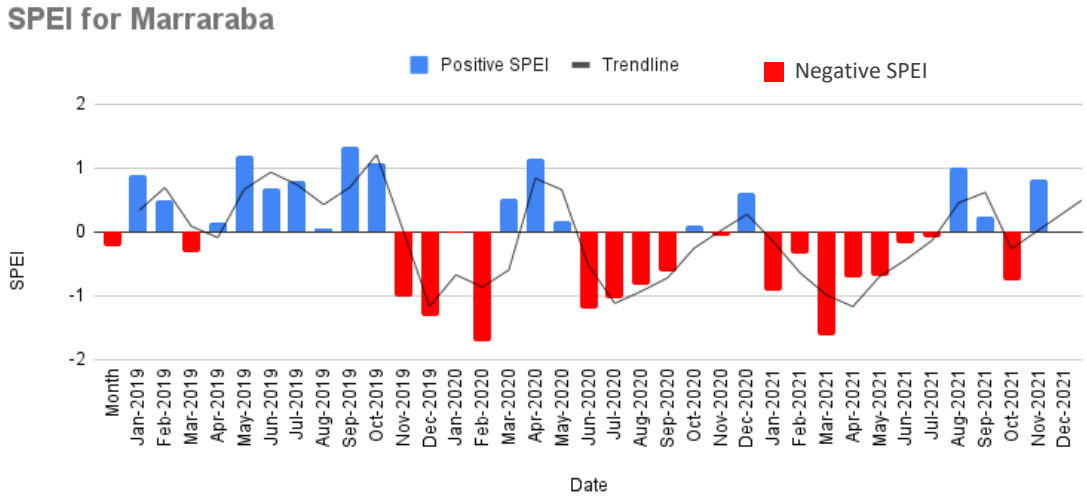

Figure (53) Estimated SPEI for Marraraba

In addition, the drought series in 2021 demonstrate a higher frequency of drought duration s compared to previous years. Moreover, the frequency of drought in 2019 was lower than that of 2020 and 2021. The drought appears to progress incrementally over the specified years.

4.3.5 Comparison Validation for Marraraba using SPEI and Groundwater Anomaly Results

Figure20 below shows a temporal comparison between groundwater and SPEI. As observed, there

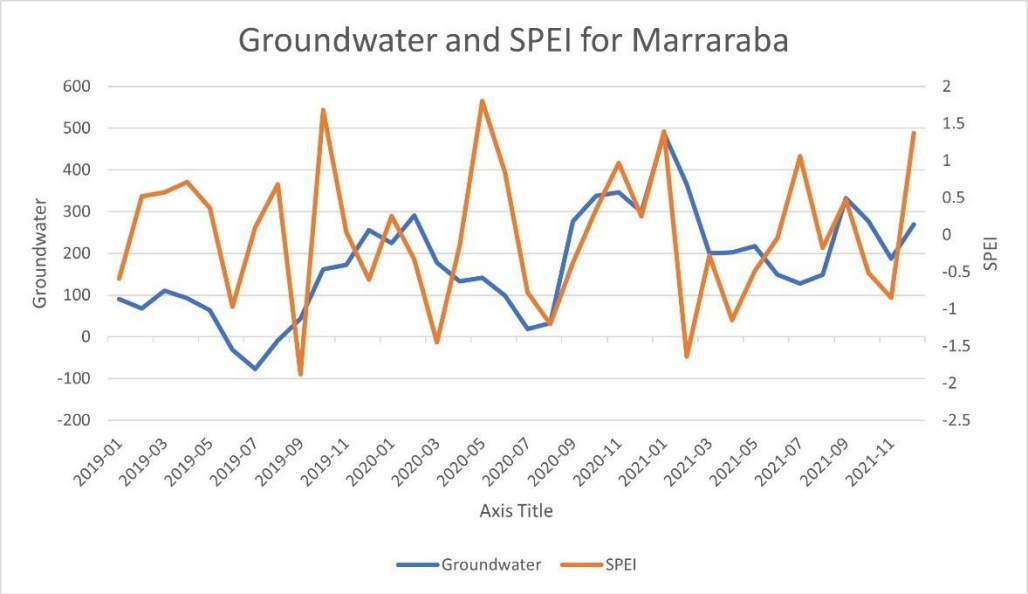

Figure (54) Marraraba. Groundwater Anomaly and SPEI

Seem to be a major similarity in velocity at the end of 2020 into the start of 2021, also noticeable is the drop in Land deformation velocity and SPEI at the second quarter of 2020. Another notable observation in both trends is the rise and drop at the end of 2021.

4.3.6 Comparison Validation for Marraraba Area1 using SPEI and Land Deformation Results

The velocity series between land deformation and SPEI in the Marraraba Area1 can be observed from Figure20. In particular, there appears to be a similarity in the temporal trend of the two variables in 2019, with both land deformation and SPEI reaching high values of 6 and 1.4, respectively, which may indicate the presence of groundwater for that particular year.

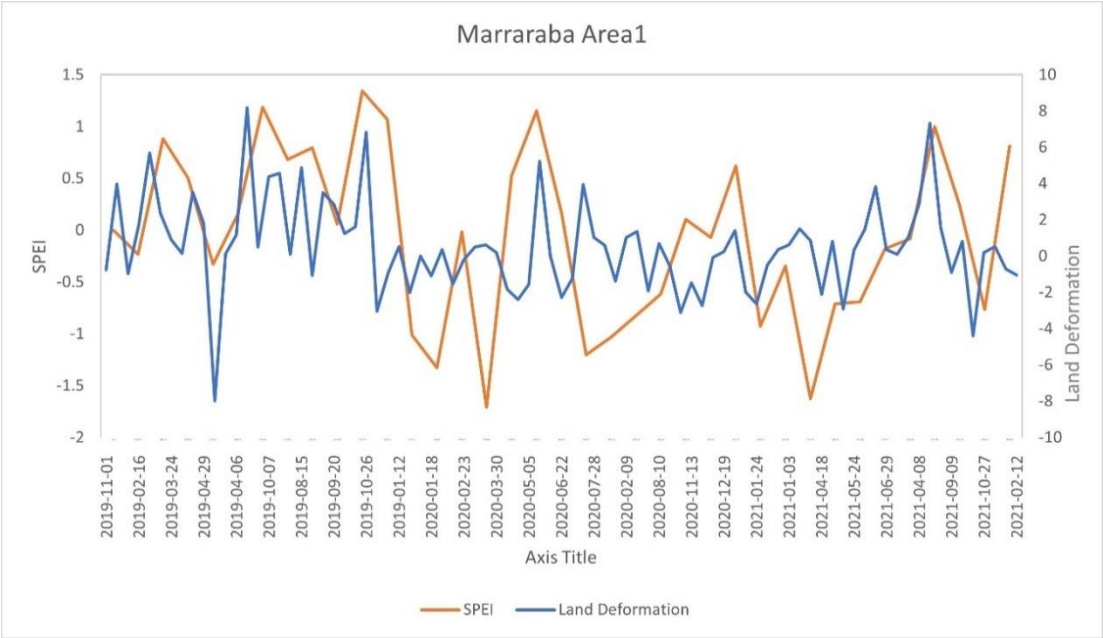

Figure (55) Marraraba Area1. Land deformation and SPEI

Major drops are also observed in early and late 2021, with SPEI value of -1.6 around February and land deformation value of -4.9 around October which suggest that groundwater is depleting in this region at the specified year.

4.3.3 Comparison Validation for Marraraba Area2 using SPEI and Land Deformation Results

Figure20 below shows a temporal trend of land deformation and SPEI for Marraraba Area2. As observed, there seem to be a similarity in trend especially in 2019 with values rising as high as 10m for land deformation and 1.3 for SPEI which suggests the presence of groundwater, and for 2020 some similarities in trend can also be observed around may with land deformation and SPEI almost rising at the same velocity, a major drop however can be observed in 2021 suggesting extreme drought for SPEI and subsidence for Land deformation which all together points to the fact that groundwater is depleting in this region in that particular year.

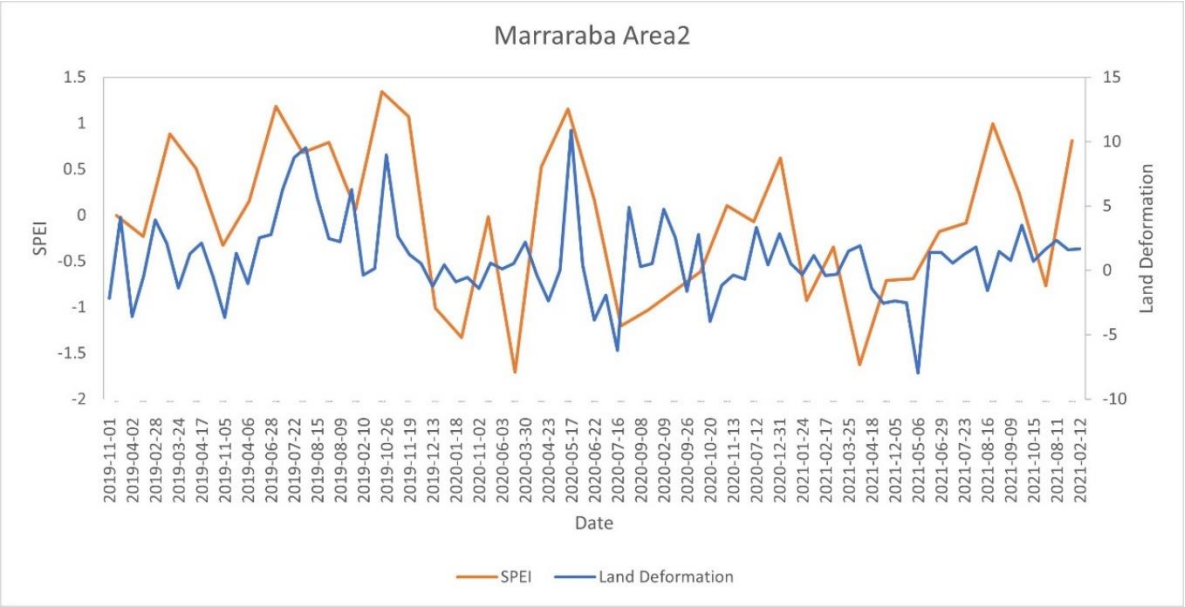

Figure (56) Marraraba Area2. Land deformation and SPEI

CHAPTER FIVE

5.0 CONCLUSION

5.1 Summary

In this study, I have used StaMPS InSAR technique for Land Deformation mapping and derived Groundwater Anomaly using GRACE and GLDAS, I have also estimated the SPEI of my study regions using temperature and precipitation in order to investigate the drought conditions respectively. All these results have been compared and observed for trend similarities. In the whole of Maiduguri, it was observed that Land Deformation and Groundwater Anomaly showed somewhat similar linear trend as seen in figure (47) which suggest the increasing presence of groundwater. Also, when Groundwater Anomaly was compared with the SPEI for Maiduguri as seen in figure (50) an observable similarity was recorded in the trends especially in 2020 and 2021, with values rising to as high as 1m and 380m for SPEI and Land deformation respectively (indicating the presence of GW) , to values dropping as low as -1.2 for SPEI and 10m for GW anomalies (indicating GW depletion).

While in Marraraba, my initial validation using Land deformation and Groundwater Anomaly appeared unjustified because, land deformation analysis only covered one-fourth of the pixel used to estimate GW anomalies, but I was able to compare the Land deformation results of Marraraba to the SPEI results of this same region and some striking similarities in trends were observed through the specified years with values rising to as high as 1m and 13m for SPEI and Land deformation respectively (indicating the presence of GW) , to values dropping as low as -1.4 for SPEI and 99m for GW anomalies (indicating GW depletion). Based on my analysis and findings, Sentinel-1 and GRACE are significant contributors to water resource management to a considerable degree. Furthermore, incorporating Climatological indices provides a more comprehensive basis for arguments and findings. However, GRACE is more suitable for regional and global scale estimations. In cases where zonal estimations are required, other indices could be utilized to reinforce findings.

Even with differences in resolution there still seem to be close trend variations in these results. However, models are not without errors and my results are not an exception, one reason is because the phenomena under investigation is a complex one, and the unavailability of in-situ data for solid validations already pose questions of uncertainties which are undeniable. However, despite the potential biases that may exist in my results, these findings are critical for informing water resource management practices. Understanding the complex interplay between these factors (Water resources, Climatology and Land Deformation) can aid in developing sustainable water resource management strategies, particularly in regions vulnerable to water scarcity and drought. While further research is

needed to improve the accuracy of these analyses, the insights gained from this project underscore the importance of continued efforts to monitor and manage our precious water resources.

5.2 Limitations

There are several limitations to this project that should be acknowledged. Firstly, in-situ data was not available for all of the study regions, this may have introduced some uncertainty in my results. The complexity of the methods applied was not a straight forward effort and required a lot of attention to detail as omitting even the thinnest step could result in errors, this was time consuming and the processing capabilities of my machine also contributed to this. Another limitation was the differences in spatial resolutions, comparing the results to have a smooth judgement was difficult.

5.3 Future Work

- My first recommendation for future project is that systems and solutions be designed in order to acquire in-situ data and collaborative participation with already established bodies would altogether aid the achievement of this.

- Downscaling GRACE is my second recommendation for future projects, as mentioned a few times in my thesis, the differences in resolution created noises or uncertainties in my results and a better resolution that can accommodate local and regional scale analysis, as this will be advantageous and produce meaningful results.

- Further statistical analysis is also required for proper validation and comprehensiveness.
- I will also recommend the identification of potential sites for groundwater extraction, since groundwater itself is not evenly distributed under the ground, solutions that can identify where they are will be a great help towards solving water crisis issues.

REFERENCES

1. Abdullin, A., & Jónsson, S. (n.d.). *Enhanced Assimilation of InSAR Displacement and Well Data for Groundwater Monitoring*.

2. Ali, Z., Hussain, I., Faisal, M., Nazir, H. M., Moemen, M. A., Hussain, T., & Shamsuddin, S. (2017). A Novel Multi-Scalar Drought Index for Monitoring Drought: The Standardized Precipitation Temperature Index. *Water Resources Management*, *31*(15), 4957–4969. https://doi.org/10.1007/s11269-017-1788-1

3. Aswathi, J., Binoj Kumar, R. B., Oommen, T., Bouali, E. H., & Sajinkumar, K. S. (2022). InSAR as a tool for monitoring hydropower projects: A review. *Energy Geoscience*, *3*(2), 160–171. https://doi.org/10.1016/j.engeos.2021.12.007

4. Bettadpur, S. (n.d.). *Satellite Gravity: GRACE & GOCE*.

5. Bohn, V. Y., Rivas, R., Varni, M., & Piccolo, M. C. (2020). Using SPEI in predicting water table dynamics in Argentinian plains. *Environmental Earth Sciences*, *79*(19), 469. https://doi.org/10.1007/s12665-020-09210-0

6. Castellazzi, P., Martel, R., Galloway, D. L., Longuevergne, L., & Rivera, A. (2016). Assessing Groundwater Depletion and Dynamics Using GRACE and InSAR: Potential and Limitations: P. Castellazzi et al. Groundwater X, no. X: XX-XX. *Groundwater*, *54*(6), 768–780. https://doi.org/10.1111/gwat.12453

7. Cazenave, A., Champollion, N., Benveniste, J., & Chen, J. (Eds.). (2016). *Remote Sensing and Water Resources* (Vol. 55). Springer International Publishing. https://doi.org/10.1007/978-3-319-32449-4

8. Collignon, B. (2020). A new tool for the remote sensing of groundwater tables: Satellite images of pastoral wells. *Open Geospatial Data, Software and Standards*, *5*(1), 4. https://doi.org/10.1186/s40965-020-00077-3

9. Delgado Blasco, J., Foumelis, M., Stewart, C., & Hooper, A. (2019). Measuring Urban Subsidence in the Rome Metropolitan Area (Italy) with Sentinel-1 SNAP-StaMPS Persistent Scatterer Interferometry. *Remote Sensing*, *11*(2), 129. https://doi.org/10.3390/rs11020129

10. Fang, Y., & Jawitz, J. W. (2019). The evolution of human population distance to water in the USA from 1790 to 2010. *Nature Communications*, *10*(1), 430. https://doi.org/10.1038/s41467-019-08366-z

11. Giao, P. H., Anh, N. T. H., & Khai, H. N. (2020). Geotechnical Characterization and Land Subsidence Analysis for the UMRT Line No.3 in Hanoi. In P. Duc Long & N. T. Dung (Eds.), *Geotechnics for Sustainable Infrastructure Development* (Vol. 62, pp. 289–296). Springer Singapore. https://doi.org/10.1007/978-981-15-2184-3_36

12. Grassi, F., & Mancini, F. (n.d.). *Sentinel-1 data for ground deformation monitoring: The SNAP-StaMPS workflow*.

13. Jipkate, A. B., Londhe, D. S., & Katpatal, Y. B. (2020). Estimation of Drought Indices for Assessing the Impact of Climatic Variables on Groundwater Fluctuation over Upper Bhima Sub Basin. *IOP Conference Series: Earth and Environmental Science*, *597*(1), 012002. https://doi.org/10.1088/1755-1315/597/1/012002

14. Khan, M. A., Zhang, X., Ali, Z., Jiang, H., Ismail, M., & Qamar, S. (2022). A New Standardized Type Drought Indicators Based Hybrid Procedure for Strengthening Drought Monitoring System. *Tellus A: Dynamic Meteorology and Oceanography*, *74*(2022), 119–140. https://doi.org/10.16993/tellusa.47

15. Liu, Z., Liu, P.-W., Massoud, E., Farr, T. G., Lundgren, P., & Famiglietti, J. S. (2019). Monitoring Groundwater Change in California's Central Valley Using Sentinel-1 and GRACE Observations. *Geosciences*, *9*(10), 436. https://doi.org/10.3390/geosciences9100436

16. Meghwal, R., Shah, D., & Mishra, V. (2019). On the Changes in Groundwater Storage Variability in Western India Using GRACE and Well Observations. *Remote Sensing in Earth Systems Sciences*, *2*(4), 260–272. https://doi.org/10.1007/s41976-019-00026-6

17. Oštir, K., & Komac, M. (2007). PSInSAR and DInSAR methodology comparison and their applicability in the field of surface deformations–A case of NW Slovenia. *Geologija*, *50*(1), 77–96. https://doi.org/10.5474/geologija.2007.007

18. Pamungkas, Y. A., & Chiang, S. H. (2021). Monitoring land subsidence induced by groundwater change using satellite gravimetry and radar interferometry measurements. Case study: Surabaya city, Indonesia. *IOP Conference Series: Earth and Environmental Science*, *916*(1), 012030. https://doi.org/10.1088/1755-1315/916/1/012030

19. Pamungkas, Y. A., & Chiang, S.-H. (n.d.). *MONITORING LAND SUBSIDENCE INDUCED BY GROUNDWATER CHANGE USING SENTINEL 1 AND GRACE SATELLITE OBSERVATIONS, CASE STUDY IN JAKARTA CAPITAL CITY*.

20. Rehman, M. A. U., & Masood, A. (n.d.). *Satellite-Based Groundwater Monitoring*.

21. Srivastava, S., & Dikshit, O. (2022). Analysis of groundwater storage (GWS) dynamics and its temporal evolution for The Indo-Gangetic plain using GRACE data. *Remote Sensing Applications: Society and Environment*, *25*, 100685. https://doi.org/10.1016/j.rsase.2021.100685

22. Stagge, J. H., Tallaksen, L. M., & Xu, C.-Y. (n.d.). *Standardized precipitation-evapotranspiration index (SPEI): Sensitivity to potential evapotranspiration model and parameters*.

23. Svoboda, M. D., & Fuchs, B. A. (2016). *Handbook of drought indicators and indices*. World Meteorological Organization.

24. Tiwari, A., Dwivedi, R., Narayan, A. B., Dikshit, O., & Singh, A. K. (2014). Efficacy of StaMPS technique for monitoring surface deformation in L'Aquila, Italy. *The International Archives of the Photogrammetry, Remote Sensing and Spatial Information Sciences*, *XL–8*, 141–145. https://doi.org/10.5194/isprsarchives-XL-8-141-2014

25. Torres, R., Snoeij, P., Davidson, M., Bibby, D., & Lokas, S. (2012). The Sentinel-1 mission and its

application capabilities. *2012 IEEE International Geoscience and Remote Sensing Symposium*, 1703–1706. https://doi.org/10.1109/IGARSS.2012.6351196

26. van der Horst, T., Rutten, M. M., van de Giesen, N. C., & Hanssen, R. F. (2018). Monitoring land subsidence in Yangon, Myanmar using Sentinel-1 persistent scatterer interferometry and assessment of driving mechanisms. *Remote Sensing of Environment*, *217*, 101–110. https://doi.org/10.1016/j.rse.2018.08.004

27. Verma, A., Kumar, A., & Kumar, S. (2016). *Analysis of groundwater anomalies using GRACE over various districts of Jharkhand* (R. Khanbilvardi, A. Ganju, A. S. Rajawat, & J. M. Chen, Eds.; p. 98770U). https://doi.org/10.1117/12.2222204

28. Vicente-Serrano, S. M., Beguería, S., & López-Moreno, J. I. (2010). A Multiscalar Drought Index Sensitive to Global Warming: The Standardized Precipitation Evapotranspiration Index. *Journal of Climate*, *23*(7), 1696–1718. https://doi.org/10.1175/2009JCLI2909.1

29. Vicente-Serrano, S. M., López-Moreno, J. I., Beguería, S., Lorenzo-Lacruz, J., Azorin-Molina, C., & Morán-Tejeda, E. (2012). Accurate Computation of a Streamflow Drought Index. *Journal of Hydrologic Engineering*, *17*(2), 318–332. https://doi.org/10.1061/(ASCE)HE.1943-5584.0000433

30. Wang, Q., Zeng, J., Qi, J., Zhang, X., Zeng, Y., Shui, W., Xu, Z., Zhang, R., Wu, X., & Cong, J. (2021). A multi-scale daily SPEI dataset for drought characterization at observation stations over mainland China from 1961 to 2018. *Earth System Science Data*, *13*(2), 331–341. https://doi.org/10.5194/essd-13-331-2021

31. Xue, D., Gui, D., Dai, H., Liu, Y., Liu, Y., Zhang, L., & Ahmed, Z. (2022). Oasis sustainability assessment in arid areas using GRACE satellite data. *Environmental Monitoring and Assessment*, *194*(5), 361. https://doi.org/10.1007/s10661-022-09929-2

32. Ye, L., Shi, K., Zhang, H., Xin, Z., Hu, J., & Zhang, C. (2019). Spatio-Temporal Analysis of Drought Indicated by SPEI over Northeastern China. *Water*, *11*(5), 908. https://doi.org/10.3390/w11050908

33. How persistent scatterer interferometry is used to predict and prevent infrastructure damage; Rose Njambi, (2022). https://up42.com/blog/how-persistent-scatterer-interferometry-is-used-to-predict-and-prevent

34. Standardized Precipitation Evapotranspiration Index (SPEI); Vicente-Serrano et al., (2010) https://www.droughtmanagement.info/standardized-precipitation-evapotranspiration-index-spei/

35. GRACE and GRACE-FO; Wikipedia, last edited, 2023 https://en.wikipedia.org/wiki/GRACE_and_GRACE-FO

36. Synthetic Aperture Radar (SAR); Dr. S. C. Liew, 2001 https://crisp.nus.edu.sg/~research/tutorial/mw.htm

37. Interferometric Wide Swath; ESA USER GUIDES; De Zan, F., & Guarnieri, A. M. (2006). https://sentinels.copernicus.eu/web/sentinel/user-guides/sentinel-1-sar/acquisition-modes/interferometric-wide-swath

38. SNAP2StaMPS_User_Manual; Jose Manuel et al., 2018
https://github.com/mdelgadoblasco/snap2stamps/blob/master/Manual/SNAP2StaMPS_User_Manual.pdf

39. TRAINING KIT – HAZA12, StaMPS: Persistent Scatterer Interferometry Processing
Case Study: Mexico City, Nov. 2019 - Nov. 2020
https://ruscopernicus.eu/portal/wpcontent/uploads/library/education/training/HAZA12_StaMPsPSI_Processing_Tutorial.pdf

40. StaMPS/MTI Manual Version 4.1b
https://homepages.see.leeds.ac.uk/~earahoo/stamps/StaMPS_Manual_v4.1b1.pdf

41. About the SPEI
https://spei.csic.es/home.html#p10

42. Standardized Precipitation Evapotranspiration Index (SPEI)
https://climatedataguide.ucar.edu/climate-data/standardized-precipitation-evapotranspiration-index-spei

43. NASA Jet Propulsion Laboratory (JPL), California institute of Technology; latest update - 2022
Measuring Earth's Surface Mass and Water Changes https://grace.jpl.nasa.gov

APPENDIX I: All realized estimations for Groundwater Anomaly, Land Deformation and SPEI

Groundwater Anomaly for Maiduguri		Groundwater Anomaly for Marraraba		SPEI for Maiduguri		SPEI for Marraraba	
Date	Groundwater	Date	Groundwater	Date	SPEI	Date	SPEI
2019-01	90.1794	2019-01	98.2916	2019-01	-0.593198	2019-01	-0.232108
2019-02	68.1524	2019-02	81.0359	2019-02	0.520169	2019-02	0.883461
2019-03	110.78	2019-03	113.873	2019-03	0.573288	2019-03	0.505667
2019-04	92.5162	2019-04	88.1803	2019-04	0.714364	2019-04	-0.328125
2019-05	64.032	2019-05	44.7947	2019-05	0.364384	2019-05	0.150955
2019-06	-31.0839	2019-06	-16.8252	2019-06	-0.969998	2019-06	1.186222
2019-07	-77.2723	2019-07	-56.8201	2019-07	0.098286	2019-07	0.681807
2019-08	-8.71456	2019-08	-2.68777	2019-08	0.681251	2019-08	0.794297
2019-09	43.3206	2019-09	93.2567	2019-09	-1.878112	2019-09	0.060483
2019-10	161.653	2019-10	214.094	2019-10	1.683868	2019-10	1.343581
2019-11	172.853	2019-11	163.42	2019-11	0.041307	2019-11	1.07107
2019-12	255.596	2019-12	229.594	2019-12	-0.600876	2019-12	-1.009631
2020-01	224.717	2020-01	197.87	2020-01	0.258199	2020-01	-1.326575
2020-02	290.559	2020-02	262.888	2020-02	-0.331497	2020-02	-0.016007
2020-03	177.414	2020-03	141.59	2020-03	-1.448825	2020-03	-1.708622
2020-04	133.342	2020-04	121.729	2020-04	-0.148432	2020-04	0.523283
2020-05	141.677	2020-05	136.874	2020-05	1.805305	2020-05	1.152749
2020-06	99.5002	2020-06	120.467	2020-06	0.846159	2020-06	0.168156
2020-07	19.2665	2020-07	53.8648	2020-07	-0.775055	2020-07	-1.203264
2020-08	32.6402	2020-08	10.0557	2020-08	-1.204262	2020-08	-1.032905
2020-09	276.648	2020-09	241.126	2020-09	-0.375471	2020-09	-0.823378
2020-10	337.786	2020-10	277.161	2020-10	0.341456	2020-10	-0.613348
2020-11	346.64	2020-11	256.203	2020-11	0.96697	2020-11	0.105739
2020-12	299.245	2020-12	218.897	2020-12	0.250823	2020-12	-0.068645
2021-01	487.579	2021-01	385.746	2021-01	1.393678	2021-01	0.620671
2021-02	365.087	2021-02	298.775	2021-02	-1.639393	2021-02	-0.92919
2021-03	200.259	2021-03	144.805	2021-03	-0.277575	2021-03	-0.346617
2021-04	202.574	2021-04	146.364	2021-04	-1.147965	2021-04	-1.625224
2021-05	217.644	2021-05	137.797	2021-05	-0.489071	2021-05	-0.711413
2021-06	148.599	2021-06	126.988	2021-06	-0.043295	2021-06	-0.691475
2021-07	127.564	2021-07	132.318	2021-07	1.058364	2021-07	-0.176621
2021-08	149.374	2021-08	120.974	2021-08	-0.177113	2021-08	-0.083011
2021-09	332.971	2021-09	296.524	2021-09	0.478849	2021-09	0.996675
2021-10	276.759	2021-10	209.533	2021-10	-0.510549	2021-10	0.238987
2021-11	187.169	2021-11	151.897	2021-11	-0.848825	2021-11	-0.765799
2021-12	270.057	2021-12	210.702	2021-12	1.373974	2021-12	0.81274

APPENDIX II: All realized Land Deformation for Maiduguri

Land Deformation for Maiduguri		Land Deformation for Maiduguri Area1		Land Deformation for Maiduguri Area2	
Date	Land Deformation	Date	Land Deformation	Date	Land Deformation
2019-01-11	-5.907749	2019-01-11	-2.430959856	2019-01-11	-3.58382505
2019-01-23	-5.1536221	2019-01-23	-3.054931167	2019-01-23	-3.69458614
2019-02-04	-4.4952853	2019-02-04	-1.175616122	2019-02-04	-2.71035375
2019-02-16	-6.6329542	2019-02-16	-2.404286578	2019-02-16	-4.1798162
2019-02-28	-3.3134993	2019-02-28	-5.469422222	2019-02-28	-4.61231701
2019-03-12	-4.0372472	2019-03-12	-0.968729911	2019-03-12	-1.55349521
2019-03-24	-2.576577	2019-03-24	-1.963637978	2019-03-24	-1.47039763
2019-04-05	-4.0879001	2019-04-05	-4.02957505	2019-04-05	-2.69108427
2019-04-17	-3.3513113	2019-04-17	-4.035311	2019-04-17	-1.43368246
2019-04-29	-1.5384873	2019-04-29	1.489802039	2019-04-29	-0.60433051
2019-05-11	-1.5303782	2019-05-11	0.87359758	2019-05-11	4.536529286
2019-05-23	-4.2475258	2019-05-23	-5.527877556	2019-05-23	-0.709704
2019-06-04	-2.3022755	2019-06-04	3.203198601	2019-06-04	-0.32132844
2019-06-16	2.0772987	2019-06-16	3.275701922	2019-06-16	9.784778714
2019-06-28	-9.85894	2019-06-28	-8.156815444	2019-06-28	-4.88045959
2019-07-10	-4.2378229	2019-07-10	-8.598231944	2019-07-10	-1.75029077
2019-07-22	-13.088996	2019-07-22	-10.26655017	2019-07-22	-11.3367633
2019-08-03	10.498401	2019-08-03	22.48576556	2019-08-03	9.505155714
2019-08-15	-0.8162257	2019-08-15	2.183385528	2019-08-15	2.546199086
2019-08-27	-5.9018072	2019-08-27	-7.108672556	2019-08-27	-0.69604289
2019-09-08	19.745734	2019-09-08	28.82029222	2019-09-08	43.84537143
2019-09-20	-1.2799637	2019-09-20	-1.856309551	2019-09-20	-0.54897842
2019-10-02	3.5376743	2019-10-02	8.662088611	2019-10-02	-2.88091451
2019-10-14	-8.6909286	2019-10-14	-46.24311389	2019-10-14	-12.2944854
2019-10-26	-3.1402678	2019-10-26	-3.870449111	2019-10-26	-2.87980592
2019-11-07	-2.8211714	2019-11-07	-4.777161	2019-11-07	-1.29609358
2019-11-19	-4.2516954	2019-11-19	-3.493843889	2019-11-19	-1.07643384
2019-12-01	-4.7637729	2019-12-01	-5.260049889	2019-12-01	-4.0431825
2019-12-13	-3.3444564	2019-12-13	-4.747452889	2019-12-13	-0.71458186
2019-12-25	-4.7777327	2019-12-25	-6.987276333	2019-12-25	-1.6287299
2020-01-18	-0.5561253	2020-01-18	0.389720262	2020-01-18	0.318312632
2020-01-30	-1.8958416	2020-01-30	-0.898194799	2020-01-30	0.577352846
2020-02-11	-2.0227663	2020-02-11	-3.629591167	2020-02-11	-1.40006973
2020-02-23	0.5170782	2020-02-23	-2.12011125	2020-02-23	2.790724071
2020-03-06	0.8525201	2020-03-06	-2.291338278	2020-03-06	0.486829143
2020-03-18	0.6994271	2020-03-18	-1.239902255	2020-03-18	0.758929514
2020-03-30	0.4197896	2020-03-30	-2.035440744	2020-03-30	-0.25550722
2020-04-11	-1.813764	2020-04-11	-5.416350222	2020-04-11	-3.07203442
2020-04-23	-0.9529993	2020-04-23	-4.314028778	2020-04-23	0.303982021
2020-05-05	-1.0264495	2020-05-05	-4.806642561	2020-05-05	-0.48099492
2020-05-29	2.9847113	2020-05-29	1.22206756	2020-05-29	1.414570843

2020-06-10	1.4862964	2020-06-10	2.056438433	2020-06-10	1.862388546
2020-06-22	4.9334531	2020-06-22	1.978984733	2020-06-22	7.5061405
2020-07-04	-3.4128526	2020-07-04	-7.537560111	2020-07-04	-3.866506
2020-07-16	-0.0420654	2020-07-16	1.660581183	2020-07-16	-1.28963438
2020-07-28	2.3682339	2020-07-28	-2.31601625	2020-07-28	1.482180899
2020-08-09	-3.2595926	2020-08-09	-5.328377722	2020-08-09	-7.37976379
2020-08-21	0.7523857	2020-08-21	-0.093193991	2020-08-21	3.406475679
2020-09-02	0.2003954	2020-09-02	-1.758606833	2020-09-02	-2.58353354
2020-09-14	-0.1352407	2020-09-14	-0.660402467	2020-09-14	-1.84670964
2020-09-26	-3.3171535	2020-09-26	-6.523910111	2020-09-26	-6.00727457
2020-10-08	-1.6355949	2020-10-08	-5.1610585	2020-10-08	-2.35938862
2020-10-20	-6.7733461	2020-10-20	-8.370821722	2020-10-20	-8.18863379
2020-11-01	-2.3351317	2020-11-01	-5.320100056	2020-11-01	-3.59130071
2020-11-13	-0.2910149	2020-11-13	-3.864137167	2020-11-13	-0.3504861
2020-11-25	-2.717709	2020-11-25	-3.761085339	2020-11-25	-4.20052214
2020-12-07	0.044298	2020-12-07	-2.713320344	2020-12-07	-2.60741129
2020-12-19	1.9195167	2020-12-19	-1.369826026	2020-12-19	1.512529024
2020-12-31	1.8229866	2020-12-31	0.730827661	2020-12-31	0.770050036
2021-01-12	1.2756398	2021-01-12	2.335027639	2021-01-12	-0.27628289
2021-01-24	0.0559063	2021-01-24	-1.763737972	2021-01-24	-2.11355254
2021-02-05	0.3918148	2021-02-05	-2.378816283	2021-02-05	-0.62838429
2021-02-17	-0.0739433	2021-02-17	-1.798241664	2021-02-17	-1.29972587
2021-03-01	2.6100114	2021-03-01	0.148832117	2021-03-01	-0.97964954
2021-03-25	2.0947749	2021-03-25	-1.301020408	2021-03-25	0.705071921
2021-04-06	3.6559267	2021-04-06	0.951772419	2021-04-06	1.827360871
2021-04-18	0.8633979	2021-04-18	-1.64618635	2021-04-18	-0.42228467
2021-04-30	5.9663202	2021-04-30	11.23904767	2021-04-30	1.634893496
2021-05-12	2.5274641	2021-05-12	-3.808948561	2021-05-12	3.8213165
2021-05-24	1.5531989	2021-05-24	-0.842470664	2021-05-24	-0.88054036
2021-06-05	2.9219951	2021-06-05	2.624695322	2021-06-05	2.121597082
2021-06-17	-1.1361115	2021-06-17	-3.7755084	2021-06-17	-4.08443493
2021-06-29	1.1952111	2021-06-29	0.997758794	2021-06-29	0.530892979
2021-07-11	-1.2656393	2021-07-11	-7.850157022	2021-07-11	-2.4427425
2021-07-23	-2.9608987	2021-07-23	-5.344111289	2021-07-23	-2.35014677
2021-08-04	2.2201503	2021-08-04	-4.937566998	2021-08-04	2.791284854
2021-08-16	10.915897	2021-08-16	-8.345710556	2021-08-16	-13.516401
2021-08-28	-3.3691345	2021-08-28	-5.147520528	2021-08-28	-5.34702471
2021-09-09	-0.4888364	2021-09-09	-2.1522896	2021-09-09	-2.06856299
2021-10-03	-5.3054548	2021-10-03	-5.806600833	2021-10-03	-3.27736843
2021-10-15	-4.5247063	2021-10-15	-12.47493739	2021-10-15	-14.2497093
2021-10-27	-2.5793636	2021-10-27	-9.338031111	2021-10-27	-3.3227347
2021-10-28	-2.0690763	2021-10-28	-9.072287	2021-10-28	-1.02550459
2021-10-29	5.5799728	2021-10-29	5.737853333	2021-10-29	-0.37989846
2021-10-30	-2.0624853	2021-10-30	-7.921825444	2021-10-30	-4.31826517

APPENDIX III: All realized Land Deformation Marraraba

Land Deformation for Marraraba		Land Deformation for Marraraba Area1		Land Deformation for Marraraba Area2	
Date	Land Deformation	Date	Land Deformation	Date	Land Deformation
2019-01-11	-2.122013892	2019-11-01	-0.75318425	2019-11-01	-2.166188473
2019-01-23	1.511364697	2019-01-23	3.96238975	2019-01-23	4.130939818
2019-02-04	-2.447723185	2019-04-02	-0.967192101	2019-04-02	-3.580471236
2019-02-16	-0.297687693	2019-02-16	1.742466975	2019-02-16	-0.428295264
2019-02-28	2.580971891	2019-02-28	5.697050375	2019-02-28	3.931470418
2019-03-12	0.458483936	2019-12-03	2.349232363	2019-12-03	2.096914173
2019-03-24	-1.282522376	2019-03-24	0.906159925	2019-03-24	-1.365455177
2019-04-05	-0.546780946	2019-05-04	0.140197563	2019-05-04	1.287052418
2019-04-17	0.478322222	2019-04-17	3.534306	2019-04-17	2.142058064
2019-04-29	-0.955822474	2019-04-29	1.808503133	2019-04-29	-0.513760736
2019-05-11	-1.657060168	2019-11-05	-7.978908875	2019-11-05	-3.632987545
2019-05-23	-0.733747158	2019-05-23	0.112759963	2019-05-23	1.341327052
2019-06-04	-0.912436415	2019-04-06	1.159000625	2019-04-06	-1.031116418
2019-06-16	4.218351265	2019-06-16	8.181666625	2019-06-16	2.524276273
2019-06-28	1.930265872	2019-06-28	0.499583863	2019-06-28	2.794479673
2019-07-10	3.467884353	2019-10-07	4.368938375	2019-10-07	6.293754636
2019-07-22	3.408176997	2019-07-22	4.558172863	2019-07-22	8.779616182
2019-08-03	1.043351273	2019-03-08	0.093170713	2019-03-08	9.536568
2019-08-15	3.113222431	2019-08-15	4.867463025	2019-08-15	5.622097182
2019-08-27	0.65929366	2019-08-27	-1.069012	2019-08-27	2.458990655
2019-09-08	-0.831312577	2019-08-09	3.49437	2019-08-09	2.235742528
2019-09-20	3.144104492	2019-09-20	2.859840275	2019-09-20	6.269236364
2019-10-02	1.739326352	2019-02-10	1.24917925	2019-02-10	-0.360101364
2019-10-14	0.407484382	2019-10-14	1.626052938	2019-10-14	0.168965727
2019-10-26	6.926944024	2019-10-26	6.828998438	2019-10-26	8.982731455
2019-11-07	1.147965411	2019-07-11	-3.047588038	2019-07-11	2.6475907
2019-11-19	-0.459638932	2019-11-19	-0.917502535	2019-11-19	1.244027278
2019-12-01	0.440332193	2019-01-12	0.53811065	2019-01-12	0.542987301
2019-12-13	-0.860176078	2019-12-13	-2.008646015	2019-12-13	-1.211620991
2019-12-25	0.249320167	2019-12-25	0.002916513	2019-12-25	0.424613555
2020-01-18	-0.107720799	2020-01-18	-1.098776563	2020-01-18	-0.8742782
2020-01-30	-0.255219161	2020-01-30	0.355598274	2020-01-30	-0.5265414
2020-02-11	-0.315220439	2020-11-02	-1.528947025	2020-11-02	-1.390395036
2020-02-23	-0.940851394	2020-02-23	-0.204633975	2020-02-23	0.56563534
2020-03-06	-0.364517397	2020-06-03	0.50137015	2020-06-03	0.118077764
2020-03-18	-0.082518648	2020-03-18	0.612447313	2020-03-18	0.5477035
2020-03-30	0.166754604	2020-03-30	0.199067463	2020-03-30	2.195307818
2020-04-11	0.4238369	2020-11-04	-1.835001063	2020-11-04	-0.369171147
2020-04-23	-1.545783622	2020-04-23	-2.397320314	2020-04-23	-2.358315755
2020-05-05	-0.744430095	2020-05-05	-1.568192054	2020-05-05	0.0039999

2020-05-17	9.826927981	2020-05-17	5.237476725	2020-05-17	10.89342109
2020-06-10	0.047770403	2020-10-06	0.004713225	2020-10-06	0.395036773
2020-06-22	-2.076165528	2020-06-22	-2.2859095	2020-06-22	-3.863094173
2020-07-04	-1.03128441	2020-04-07	-1.241122763	2020-04-07	-1.910843782
2020-07-16	-5.868649791	2020-07-16	3.951359088	2020-07-16	-6.225050636
2020-07-28	0.324848955	2020-07-28	1.026154638	2020-07-28	4.902577655
2020-08-09	0.386546549	2020-09-08	0.597537388	2020-09-08	0.294439791
2020-08-21	-0.709229231	2020-08-21	-1.373352013	2020-08-21	0.533860258
2020-09-02	1.014369405	2020-02-09	1.02599071	2020-02-09	4.757005455
2020-09-14	1.799735525	2020-09-14	1.365794275	2020-09-14	2.535276164
2020-09-26	0.662838171	2020-09-26	-1.923346675	2020-09-26	-1.595599882
2020-10-08	2.711794243	2020-08-10	0.695191125	2020-08-10	2.784315818
2020-10-20	-1.364279584	2020-10-20	-0.540500863	2020-10-20	-3.975836136
2020-11-01	-1.012280406	2020-01-11	-3.119309175	2020-01-11	-1.170693636
2020-11-13	-0.102017881	2020-11-13	-1.463540888	2020-11-13	-0.355526661
2020-11-25	0.075993755	2020-11-25	-2.730270238	2020-11-25	-0.658617706
2020-12-07	1.587132401	2020-07-12	-0.0730363	2020-07-12	3.333583327
2020-12-19	-0.106346363	2020-12-19	0.23859645	2020-12-19	0.442423591
2020-12-31	1.655810665	2020-12-31	1.404858096	2020-12-31	2.836992727
2021-01-12	0.895042217	2021-12-01	-1.985455625	2021-12-01	0.538787066
2021-01-24	-0.539615064	2021-01-24	-2.641890263	2021-01-24	-0.328187512
2021-02-05	0.671581417	2021-05-02	-0.503547313	2021-05-02	1.162500909
2021-02-17	0.153151095	2021-02-17	0.364323374	2021-02-17	-0.3940726
2021-03-01	0.192202511	2021-01-03	0.616330356	2021-01-03	-0.287651746
2021-03-25	0.259823322	2021-03-25	1.498778075	2021-03-25	1.499081018
2021-04-06	0.801207356	2021-06-04	0.869378163	2021-06-04	1.934644636
2021-04-18	-0.869245823	2021-04-18	-2.101143625	2021-04-18	-1.412564391
2021-04-30	-0.761988569	2021-04-30	0.820651613	2021-04-30	-2.552694636
2021-05-12	-2.912738136	2021-12-05	-2.926248413	2021-12-05	-2.360603773
2021-05-24	0.740085999	2021-05-24	0.332294225	2021-05-24	-2.5185183
2021-06-05	-3.262199737	2021-05-06	1.472666395	2021-05-06	-7.955796
2021-06-17	1.906656117	2021-06-17	3.842678888	2021-06-17	1.400369282
2021-06-29	0.1699488	2021-06-29	0.360431875	2021-06-29	1.393080273
2021-07-11	0.931044346	2021-11-07	0.108226	2021-11-07	0.577544327
2021-07-23	1.418896219	2021-07-23	1.061209639	2021-07-23	1.262946418
2021-08-04	2.204311672	2021-04-08	2.889718163	2021-04-08	1.812515018
2021-08-16	4.301820304	2021-08-16	7.332306	2021-08-16	-1.579595091
2021-08-28	3.519244203	2021-08-28	1.571389413	2021-08-28	1.474831527
2021-09-09	0.607935185	2021-09-09	-0.889452038	2021-09-09	0.774457055
2021-10-03	3.533204078	2021-03-10	0.814635288	2021-03-10	3.496589645
2021-10-15	0.053196836	2021-10-15	-4.382606538	2021-10-15	0.704710536
2021-10-27	1.39777665	2021-10-27	0.204182354	2021-10-27	1.598218409
2021-11-08	1.856658777	2021-08-11	0.524340075	2021-08-11	2.345829627
2021-11-20	0.421258912	2021-11-20	-0.714183813	2021-11-20	1.624639709
2021-12-02	0.532875759	2021-02-12	-1.034216219	2021-02-12	1.670808918